Journal of Hydrology: Regional Studies 34 (2021) 100795

Contents lists available at ScienceDirect

Journal of Hydrology: Regional Studies

journal homepage: www.elsevier.com/locate/ejrh

Decadal and multidecadal natural variability of African rainfall

Horst-Joachim Lüdecke [a], Gisela Müller-Plath [b], Michael G. Wallace [c], Sebastian Lüning [d,*]

[a] University of Applied Sciences HTW, Saarbrücken, Germany
[b] Technische Universität Berlin, Berlin, Germany
[c] Michael Wallace & Associates, Albuquerque, NM, USA
[d] Institute for Hydrography, Geoecology and Climate Sciences, Hauptstraße 47, 6315, Ägeri, Switzerland

ARTICLE INFO

Keywords:
Precipitation
Natural variability
Modes of variability
Sahel
Atlantic Multidecadal Oscillation
North Atlantic Oscillation
Indian Ocean Dipole
Solar forcing
Floods
Droughts

ABSTRACT

Study region: Africa
Study focus: African rainfall shows significant year-to-year natural fluctuations that in part are linked to teleconnections associated with modes of variability in the Atlantic, Pacific and Indian oceans. A better understanding of African rainfall variability and potential drivers would help to better prepare African societies for anticipated droughts and floods by taking early precautionary action. Here we are presenting the first continent-wide analysis of African rainfall variability on a month-by-month and country-by-country basis. We have calculated Pearson r values for smoothed monthly rainfall data of 49 African countries over the period 1901–2017 which we compared to six potential climatic drivers of natural variability, namely AMO, NAO, ENSO (El Niño Southern Oscillation), Pacific Decadal Oscillation (PDO), Indian Ocean Dipole (IOD) and solar activity changes. We allowed time lags of up to 11 months for each potential driver (66 months for solar activity).
New hydrological insights for the region: The dynamic temporal-spatial evolution of the seasonal Pearson correlations was mapped out across the continent, tracking the gradual or abrupt expansion, displacement and subsequent waning of the various effects over the course of the year. Relationships are complicated by characteristic time lags, non-stationary correlations and occasional phase shifts. Our empirical results may help to further improve short- to midterm rainfall prognoses in Africa and provide important calibration data for the further improvement of climate models.

1. Introduction

African rainfall varies significantly on year-to-year to multi-decadal time-scales. In some years an over-abundance of rain causes dangerous floods, whilst in other years the same region may suffer from drought conditions. Water forms the basis for life, as it provides both drinking water and irrigation for agricultural food production. Water resources management and protection efforts against hydrological natural hazards require a good understanding of natural variability of rainfall and its potential drivers. Significant efforts have been made over the past 25 years to unravel the systematics behind African rainfall dynamics and its relation with oceanic

* Corresponding author.
E-mail addresses: moluedecke@t-online.de (H.-J. Lüdecke), gisela.mueller-plath@tu-berlin.de (G. Müller-Plath), mwa@abeqas.com (M.G. Wallace), luening@ifhgk.org (S. Lüning).

https://doi.org/10.1016/j.ejrh.2021.100795
Received 7 August 2020; Received in revised form 15 February 2021; Accepted 17 February 2021
Available online 26 February 2021

modes of variability in combination with anthropogenic and other natural forcings (e.g. Nicholson, 2000, 2014). Some of the first-order influence factors are now well known. For example, the negative phase of the North Atlantic Oscillation (NAO) normally leads to increased rainfall in Morocco (Lamb and Peppler, 1987), the positive phase of the Atlantic Multidecadal Oscillation (AMO) results in above-average rainfall in the Sahel zone (Zhang and Delworth, 2006), and La Niña (negative El Niño Southern Oscillation, ENSO) is typically associated with drought conditions in parts of East Africa (Lott et al., 2013).

It has also been recognized that relationships between rainfall and oceanic modes of variability differ greatly from region to region and from season to season. Different variability indices influence rainfall during different times of the year. A time-dependent, non-stationary character is symptomatic for many of the observed relations (Nicholson, 2017). Correlations that were strong over several

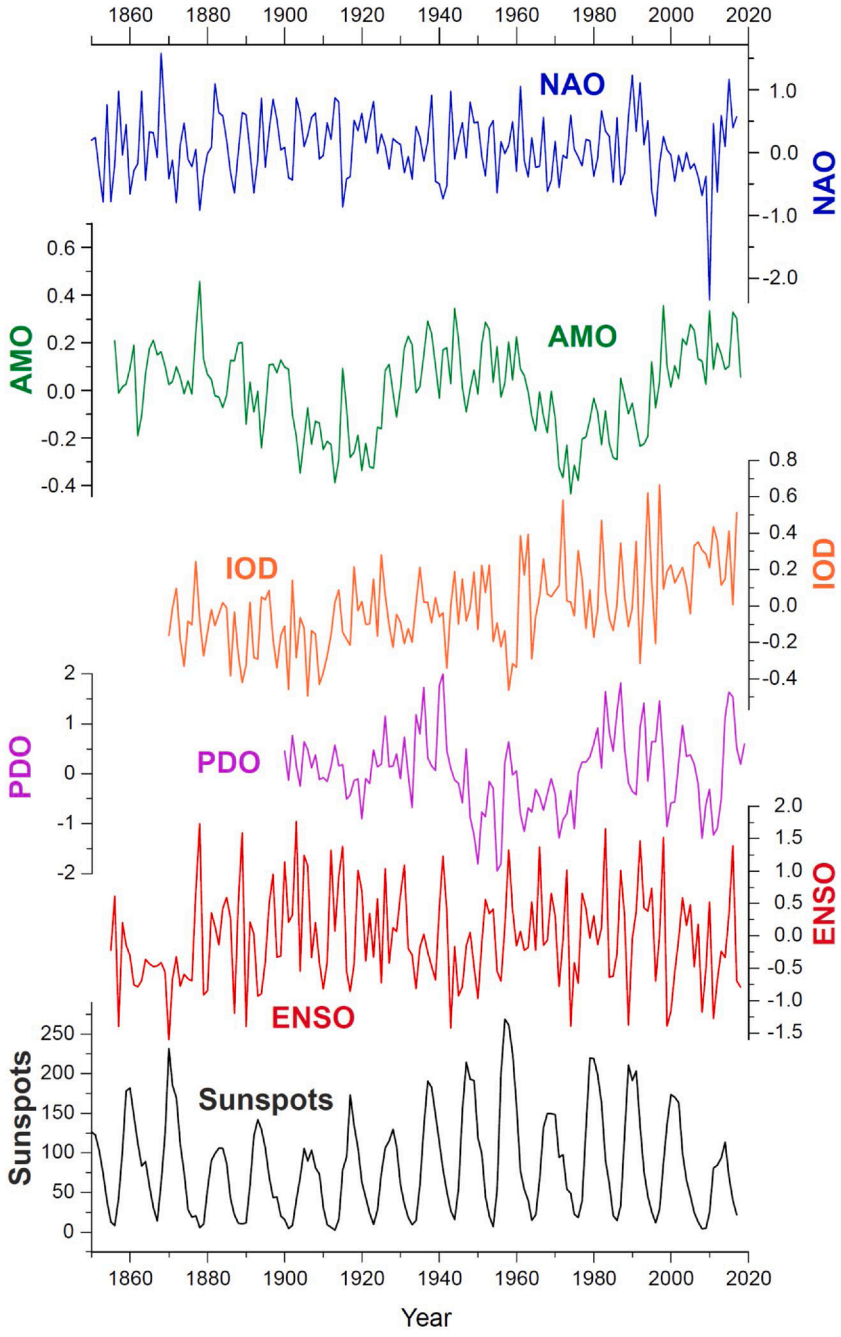

Fig. 1. Time Series of NAO, AMO, IOD, PDO, ENSO and Sunspots during the last 160 years. Shown are annual mean values, unsmoothed. Please note that the unsmoothed annual values shown here serve only for illustration purposes and were not used in the correlational analysis. Examples of monthly time series smoothed by using a Savitzky-Golay filter are shown in Figs. S7-S18.

decades may suddenly weaken or disappear. Occasional phase reversals as well as multi-months to multi-year time lags between climatic triggers and rainfall add further complexity.

In this contribution we are attempting to identify the most important correlations of rainfall with six potential climatic drivers of natural variability, namely AMO, NAO, ENSO, Pacific Decadal Oscillation (PDO), Indian Ocean Dipole (IOD) and solar activity changes ("SUN"), regionally mapped out across Africa, separately for all 12 months of the year. The trend mapping is based on lag-optimized Pearson r values that were calculated for monthly rainfall over the period 1901–2017 for 49 African countries. The monthly analysis has been shown to be particularly sensitive to seasonally variable influences of potential climatic drivers on rain (Laurenz et al., 2019) and temperature (Lüdecke et al., 2020). Although not used much in the recent past, the method reaches back to Ogallo (1988) who found monthly rainfall in East Africa highly correlated with lag zero Southern Oscillation Index (SOI).

Our empirical results may help to improve short- to midterm rainfall prognoses in Africa and provide important calibration data for the further improvement of climate models. In many cases, simulations still struggle to replicate the observed rainfall trends (e.g. MacKellar et al., 2014; Masih et al., 2014; Nouaceur and Murarescu, 2016; Rowell et al., 2015).

2. Hydroclimate of Africa and rainfall trends

Large parts of North Africa, southern Africa and the Horn of Africa are dominated by hot, arid desert and steppe climates (Köppen, 1918). The equatorial region of Africa has humid tropical climates, whilst parts of southern Africa are under the influence of temperate climates. As part of the yearly monsoon cycle, the rain belt moves from West Africa and the Sahel in boreal summer to southern Africa in austral summer. In equatorial coastal East Africa there are two rainy seasons, namely the 'long rains', which occur between March and May, and the 'short rains', which start in September and peak in October and November. Although the daily mean rainfall during the short rains is lower than that during the long rains, the short rains exhibit greater interannual variability (Black, 2005). There are also two rainy seasons along the Gulf of Guinea coast (January-March and July-September). The southwestern tip of South Africa receives rain in austral winter.

Only a few significant long-term rainfall trends are evident in Africa over the past decades and century (Nicholson et al., 2018). West Africa and the Sahel experienced severe droughts during the 1970s and 1980s with a regime shift towards increased rainfall around 1992 (Badou et al., 2017; Park et al., 2016). Different trends were reported from equatorial eastern Africa for the short and long rainfall seasons (Cattani et al., 2018; Gitau et al., 2017). There are no trends in regionally aggregated rainfall in South Africa (MacKellar et al., 2014). The African hydroclimatic variability during the last 2000 years was compiled by Nash et al. (2016). Lüning et al. (2018) mapped out changes in African rainfall during the Medieval Climate Anomaly (MCA, 1000–1200 AD).

3. Elements of natural rainfall variability

Africa is the second largest continent in the world and is surrounded by oceans, except for the Sinai land bridge to Asia. African rainfall is believed to be influenced by a very complex mix of drivers associated with oceanic modes of variability of the Atlantic (NAO, AMO), Indian Ocean (IOD) and the Pacific (PDO, ENSO) (Diatta and Fink, 2014; Mpelasoka et al., 2018; Nicholson and Kim, 1997) (Fig. 1) as well as solar activity changes (e.g. van Loon et al., 2004). In the following sections 3.1 to 3.7 we are summarizing previously reported relationships between rainfall and natural drivers. In addition to natural drivers, precipitation is also thought to be influenced by anthropogenic drivers (e.g. Lott et al., 2013; Otto et al., 2018) which however are outside the scope of this contribution for reasons of focus and length.

3.1. North Atlantic Oscillation (NAO)

The NAO was discovered through several studies in the late 19th and early 20th centuries (see overview in Stephenson et al., 2003) and is based on the surface sea-level pressure difference between the subtropical Azores High and the subpolar Icelandic Low (Hurrell et al., 2003). Boreal winter rainfall in Morocco and northwestern Algeria is negatively correlated with the NAO (Knippertz et al., 2003a; Lamb and Peppler, 1987; Marchane et al., 2016; Taibi et al., 2017). In contrast, winter rainfall in Libya and northern Egypt has been reported to be positively correlated with the NAO (Brandimarte et al., 2011; López-Moreno et al., 2011). On seasonal-interannual timescales, the rainfall in northwestern Africa can be influenced by a North Atlantic sea surface temperature (SST) tripole, and the influence may be asymmetric with respect to the sign of the SST and also seasonally dependent (Li et al., 2003). Boreal winter rainfall in Uganda shows negative correlations with the NAO (McHugh and Rogers, 2001). The West African summer monsoon rainfall is negatively correlated with boreal spring NAO (Li et al., 2012).

3.2. Atlantic Multidecadal Oscillation (AMO)

The AMO was first described by Schlesinger and Ramankutty (1994) and represents a low-frequency ocean cycle with an estimated period of 60–80 years (Kerr, 2000). The AMO is based upon the average anomalies of SST in the North Atlantic basin between 0−60 °N from which the long-term warming signal is removed by detrending (Trenberth and Shea, 2006). The Sahel boreal summer rain is strongly positively correlated with the AMO (Berntell et al., 2018; Diatta and Fink, 2014; Folland et al., 1986; Martin et al., 2014; O'Reilly et al., 2017; Shanahan et al., 2009; Zhang and Delworth, 2006; Zhang et al., 2019). A negative correlation of boreal summer/autumn rainfall and AMO was reported for central equatorial Africa (Diem et al., 2014). Martin and Thorncroft (2014) published rainfall maps which show positive AMO correlations along the Atlantic coast in October-December (OND) and in East Africa in

January-March (JFM). Negative AMO correlations were reported by these authors for the southeastern African Indian Ocean coastline and Madagascar. Taye and Willems (2012) suggested a positive correlation of Ethiopian rainfall during the dry season (October-May) with AMO.

3.3. Indian Ocean Dipole (IOD)

The Indian Ocean Dipole (IOD) is defined as the difference between the SST in the western and eastern equatorial Indian Ocean (Saji et al., 1999). The IOD is linked to ENSO through an extension of the Walker Circulation to the west and associated Indonesian Throughflow. The short rain season in East Africa in October to December (OND) is strongly positively correlated to the IOD (Black, 2005; Black et al., 2003; Clark et al., 2003; Liebmann et al., 2014; Marchant et al., 2007; Saji et al., 1999; Ummenhofer et al., 2009). It is thought that the IOD alters the local Walker circulation (Tierney et al., 2013). Floods in East Africa are more frequent during the positive phase of the IOD (Ogwang et al., 2015), whilst droughts are more common when the IOD turns negative (Lim and Hendon, 2017; Mpelasoka et al., 2018). The long rain season in East Africa in March to May (MAM) is not significantly correlated with the IOD (Owiti et al., 2008).

A positive IOD typically boosts September-November rainfall not only in East Africa, but also in a wide corridor towards the Angolan Atlantic coast as well as in western West Africa (Bahaga et al., 2015; Behera et al., 2005). At the same time, rainfall in Central Africa and southeastern Africa is suggested to be reduced, pointing to the existence of IOD dipoles (Bahaga et al., 2015; Behera et al., 2003). Positive IOD correlations have been reported in southern Africa for the austral spring-summer transition (October-December), although the correlation is non-stationary and apparently deteriorated significantly after 1997 (Manatsa et al., 2012). In the majority of southern Africa, peak rainfall occurs in the austral summer (December-February) whereby precipitation is influenced by a complex interaction of IOD with ENSO (Manatsa and Mukwada, 2012; Reason, 2001). According to Hoell et al. (2017) the phase of the IOD can disrupt or enhance the southern Africa precipitation response to ENSO, depending on whether IOD and ENSO are in the same or opposite phases. A weakly negative correlation with IOD has been reported for the boreal summer rain in the westernmost Sahel zone (Diatta and Fink, 2014).

3.4. Pacific Decadal Oscillation (PDO)

The Pacific Decadal Oscillation (PDO) is a long-lived El Niño-like oscillatory pattern of climate variability based on switching ocean temperature anomalies in the northeast and tropical Pacific Ocean (Mantua et al., 1997). In the 20th century the oscillation had two general periodicities, one from 15 to 25 years, and the other from 50 to 70 years (Mantua and Hare, 2002). Boreal summer rainfall in Ethiopia (Taye and Willems, 2012), the Sahel (Diatta and Fink, 2014; Mohino et al., 2011; Ogou et al., 2019) and the Gulf of Guinea coast (Diatta and Fink, 2014) is negatively correlated with the PDO.

3.5. El Niño–Southern Oscillation (ENSO)

The El Niño-Southern Oscillation (ENSO) is a naturally occurring phenomenon in which central and eastern equatorial Pacific SST fluctuate between two states, namely warmer (El Niño) and colder (La Niña). ENSO is attributed to have complex effects on African rainfall that differ greatly regionally and seasonally (Kiladis and Diaz, 1989; Mason and Goddard, 2001; Nicholson and Kim, 1997; Ropelewski and Halpert, 1987). Several authors have reported negative ENSO correlations with rainfall in Morocco, Northwest Algeria and Tunisia (Knippertz et al., 2003b; Meddi et al., 2010; Ouachani et al., 2013; Rodó et al., 1997; Zeroual et al., 2016). However, other studies struggled to document significant ENSO correlations in Northwest Africa (e.g. Bougara et al., 2020), probably because the coupling between ENSO and rain has repeatedly weakened over a few decades (Knippertz et al., 2003b), and because some of the correlations involved time lags of 2 years (Ouachani et al., 2013). According to Biasutti (2019) Sahel rain reduces during El Niño phases. Influence of ENSO on rainfall in West Africa is complex (Dezfuli and Nicholson, 2013). The same SST pattern may enhance rainfall in one season but reduce it in the following season (Balas et al., 2007). Discharge of the Congo River - as a comprehensive integrator of rainfall over Central Africa - is reported to be weakly and negatively correlated with ENSO (Amarasekera et al., 1997).

Summer rainfall in Ethiopia is negatively correlated with ENSO (Abtew et al., 2009; Eltahir, 1996; Korecha and Barnston, 2007; Segele et al., 2009; Zaroug et al., 2014), except in the easternmost part of the country and Somalia from where a positive ENSO correlation has been reported (Funk, 2011; Hutchinson, 1992; Korecha and Barnston, 2007). Rains in East Africa are correlated both positively (Hoell et al., 2014; Lott et al., 2013; Lyon and DeWitt, 2012) and negatively (Funk et al., 2018; Indeje et al., 2000) with ENSO, depending on the region and season. Rainfall partly lags by 1 year (Indeje et al., 2000). The ENSO correlation of the East African short rains in October-December (OND) is highly time-dependent over the past 140 years with an alternation of multidecade intervals of good and poor correlations (Clark et al., 2003; Nicholson, 2015). Rainfall modulation in the region is typically dependent on both ENSO and IOD (Hoell and Funk, 2014). Austral summer rainfall in southern Africa is negatively correlated with ENSO, interacting with the IOD (Funk et al., 2018; Hoell et al., 2015, 2017; Kane, 2009). In contrast, austral winter rain in South Africa shows a positive ENSO correlation (Philippon et al., 2012).

3.6. Solar activity changes

Solar correlations to African rainfall have been reported on time scales ranging from decadal to multi-centennial. The solar Schwabe cycle (11 years) was identified in East African (Gachari et al., 2014), Central African (van Loon et al., 2004) and South African

(Currie, 1993) rainfall, as well as in lake level changes in Lake Victoria (Alexander et al., 2007). The solar magnetic Hale cycle (22 years) is manifested in hydrometeorological data of South Africa (Alexander, 2005; Alexander et al., 2007). According to Mason and Tyson (1992) the solar effect on rainfall in southern Africa is modulated by the phase of the Quasi-Biennial Oscillation (QBO). The solar Gleissberg cycle (90 years) was found in the Nile discharge (Ruzmaikin et al., 2006). The solar Suess-de Vries cycle (200 years) occurs in both Nile discharge and Moroccan palaeohydroclimate (Ait Brahim et al., 2018; Ruzmaikin et al., 2006). Other multi-centennial solar effects on Holocene rainfall were suggested for East Africa (Hennekam et al., 2014; Junginger et al., 2014; Stager et al., 2003; Verschuren et al., 2000) and southern Africa (Heine and Völkel, 2011). Since solar activity influences most oceanic modes of variability, it therefore likely contributes indirectly in a non-linear way to changes in African rainfall. A link to solar activity changes has been reported for NAO (Helama and Holopainen, 2012; Kodera, 2002; Thiéblemont et al., 2015), AMO (Knudsen et al., 2014; Malik et al., 2018; Muthers et al., 2016; Otterå et al., 2010; Wang et al., 2017a), IOD (Kodera et al., 2007; Nugroho, 2007), PDO (Maruyama et al., 2017; Yamakawa et al., 2016), and ENSO (Huo and Xiao, 2016; Kirov and Georgieva, 2002; Kodera, 2005; Wallace, 2019).

3.7. Volcanic activity

Haywood et al. (2013) suggested that sporadic volcanic eruptions in the Northern Hemisphere strongly influenced the Atlantic SST gradient and caused Sahelian drought. Three of the four driest Sahelian summers between 1900–2010 were apparently preceded by substantial Northern Hemisphere volcanic eruptions (Haywood et al., 2013).

3.8. Interdependence of drivers

The potential drivers of African precipitation are physically not fully independent. A large body of research is devoted to how and with what time lag they interact with each other and with other atmospheric and oceanic events (Li et al., 2013; Wyatt et al., 2012). However, such considerations are beyond the scope of this paper. In the methods section of our paper, we briefly address the question of whether statistical intercorrelations are present that could affect the interpretation of the bivariate correlations between each potential driver and rainfall in African countries, as analyzed in this paper.

4. Material and methods

4.1. Data

Monthly rainfall data for 49 African countries covering the period 1901–2017 were downloaded from the Climatic Research Unit (CRU) of the University of East Anglia (dataset CRU CY v4.02 Country Averages: PRE). The monthly NAO data were sourced from the CRU, the AMO and IOD data from NOAA, and PDO and ENSO data from the KNMI Climate Explorer. The solar activity data (SUN) is based on Sunspot Number Version 2.0 from the Royal Observatory of Belgium in Brussels, Sunspot Index and Long-term Solar Observations (SILSO, Clette et al., 2015). Web addresses and dates of access are listed in Supplement chapter 2.

4.2. Statistical processing

4.2.1. Preprocessing

In order to limit the influence of outliers, we smoothed the monthly series of both the precipitation and the potential drivers using a Savitzky-Golay Filter (SGF). The SGF is a method of filtering the data for increasing the signal-to-noise ratio. The fundamental method is mathematical convolution (Riley et al., 2006) by fitting successive subsets of close-by data points with a polynomial by the linear least squares method (Luo et al., 2005; Savitzky and Golay, 1964). The SGF used here has a frame size of 11 and a polynomial order of 5. Please note that the simple moving average (SMA) of e.g. 3 months, which is frequently used for smoothing, was not appropriate in our approach, as we focused on monthly time series. Fig. S19 shows a smoothed and an unsmoothed time series for comparison.

4.2.2. Effect assessment

The effect of each potential driver NAO, AMO, IOD, PDO, ENSO and SUN on the monthly precipitation in each country was assessed with lag-optimized linear least-squares-regression. The rainfall series of each month in each country across the $N = 117$ years was linearly predicted from the monthly values of the potential driver that preceded the rainfall by 0, 1, …, 11 months (i.e., lagged it by 0, …, -11 months). Please note that "predicted" and "prediction" are used here solely in terms of the general linear model (GLM) and must not be confused with “forecasts". The absolute maximum linear correlation $|r|$ was recorded together with its sign (+ or -) and the respective time lag, and served as a measure of the positive or negative impact of this potential driver in this month and country. For SUN, the optimization ran across lags of up to -66 months, i.e. about half a Schwabe cycle.

4.2.3. Significance testing

In order to ascertain the statistical reliability of the maximized $|r|$ values, we needed the distribution of these values under the null hypothesis (H_0), stating that for all lags, i.e. 0 to -11 for NAO, AMO, IOD, PDO, ENSO, and 0 to -66 for SUN, rainfall and potential driver are uncorrelated. For each month and each driver, we generated 10.000 Monte Carlo (MC) rainfall series under H_0 by independently drawing $N = 117$ random values from a standard normal distribution (note that mean and standard deviation do not matter because the correlation is invariant under linear transformation). The normality assumption was justified by the observation that the real

monthly rainfall series across the years 1901–2017 showed almost no autocorrelation: The mean of Hurst exponents was H = 0.52, σ = 0.06, denoting nearly white noise (Kantelhardt et al., 2001). Each MC rainfall series was then subjected to the same analysis as the real data, i.e., smoothed with the SGF and linearly correlated with the same set of lags of the driver under consideration. The maximum absolute correlation $|r_{MC}|$ across the lags was recorded. For each month, each country and each driver, we rejected H_0 at significance level $p < 0.05$, $p < 0.01$ or $p < 0.001$, if the empirical $|r|$ exceeded the 0.95-,0.99- or 0.999-quantile of the respective $|r_{MC}|$ distribution. Note that these upper quantiles of $|r_{MC}|$ served as critical $|r|$ values for maximum positive as well as negative r because the random variable r_{MC} is symmetrically distributed about zero. To avoid any filter artefacts, we repeated all correlation calculations and significance tests for the unsmoothed data.

Table 1 shows the range of critical $|r|$ values obtained for all months and potential drivers, both for smoothed and unsmoothed data. Although effect sizes were larger for the smoothed data, significance decisions turned out to be more conservative because the MC-simulated random rainfall series had to be smoothed in the same way. Thus, the original data yielded even more significant results. Whilst the main paper is based on the smoothed data, a comparative analysis of smoothed and unsmoothed data can be found in the Supplement (Table S7, Figs. S19, S20).

4.2.4. Alternative significance testing

The MC method requires specifying a distribution from which N random values are drawn in each run. Due to the lack of autocorrelation, we assumed normality. However, some empirical rainfall distributions were markedly skewed, e.g. for Ethiopia in February. To validate our MC significance tests, we carried out a bootstrapping test (Efron and Tibshirani, 1993) for 11 exemplary cases. From these, only 4 were found significant ($p < 0.05$) with the MC method but 9 with the bootstrap method. In particular, every MC significance was confirmed by bootstrap but not vice versa. We are therefore confident that the normality assumption in our MC simulations has not systematically inflated the false-positive rate, but rather resulted in too conservative decisions.

4.2.5. Multiple tests

With 12 months, 49 countries and 6 potential drivers, i.e. altogether 3528 significance tests at a local significance level of $p < 0.05$, 0.05, or 0.001, we are well aware that probably a certain amount of false positives are among our results. The only remedy would be to lower the individual significance level so much that the probability of even a single false positive was less than 5%, or that the rate of false positives was limited. However, all available correction routines for multiple tests inflate the false negative rate, and this even more the stronger the tests are interdependent (McDonald, 2014: 257–261). In the present research, not only tests for consecutive months but also for neighbouring countries are highly interdependent. The false-positive rate is therefore likely to be much lower than the local significance level multiplied with the number of tests, and the false-negative rate would increase excessively if corrected. Since this is a continent-wide exploratory, hypothesis-generating study, we decided against a correction and would like to emphasize, as a precaution, that the present results will require detailed confirmation in future research

4.2.6. Interdependence of drivers

The six potential drivers considered here are not fully independent. For every rainfall series, we computed a 6 × 6 – correlation matrix of the six drivers, each with the lag that was found to optimize the linear prediction (correlation) of the rainfall in the respective country and month. With 49 countries x 12 months, we obtained 588 unsmoothed and 588 smoothed correlation matrices. Correlations were mostly spurious. In some cases, however, substantial linear relationships between drivers could be observed, in particular in cases in which more than one driver significantly predicted the rainfall. Exemplary correlation matrices are shown in the Supplement Tables S14-S17. However, in none of the cases a significant r value between the rainfall series and a driver was exceeded by an r value between two drivers.

Statistical intercorrelations between drivers do not question the interpretation of the bivariate correlations between drivers and rainfall, as mapped out and discussed in the present paper. Notably, we do not interpret our r values as indicators of direct causal physical effects. However, they do point to relationships that are practically relevant for forecasting rainfall and theoretically worth further physical analysis. Mediating, moderating, and suppressing effects need to be investigated in future work so that more complex models can be built. However, this is beyond the scope of the present paper.

Table 1
Range of the 0.95-, 0.99-, 0.999-quantiles of the $|r_{MC}|$ distributions simulated under H_0, separately for monthly series smoothed with the SGF and without (see text). Please note that the intervals in this table serve only as an overview. For significance testing, the individual quantiles obtained for each driver and month were used as critical |r | values, as listed in Table S13.

		quantile of simulated distribution of $\|r_{MC}\|$ (significance level)		
		0.95 ($p < 0.05$)	0.99 ($p < 0.01$)	0.999 ($p < 0.001$)
NAO, AMO, IOD, PDO, ENSO	**with SGF**	**0.354–0.400**	**0.424–0.473**	**0.500–0.560**
	without SGF	0.229–0.265	0.275–0.307	0.326–0.376
SUN	**with SGF**	**0.403–0.413**	**0.475–0.487**	**0.547–0.567**
	without SGF	0.266–0.273	0.312–0.320	0.357–0.382

4.3. Visualization of results

The Tables S1−S6 in the Supplement show all 3528 lag-optimized linear correlation coefficients *r* together with the respective lag information calculated for the six potential rainfall drivers in 49 countries and 12 months of the year. All $|r|$ values exceeding the $p < 0.05$ significance level for the respective driver and month are highlighted in red (positive *r*) or blue colour (negative r). Even though Table 1 provides only the interval in which the individually obtained critical r values for the 6 drivers and 12 months lie, it can be used to evaluate which correlations exceed a more rigorous significance level ($p < 0.01$ oder $p < 0.001$): With the upper bounds of the critical r-intervals given in Table 1, one is on the safe side for all countries and months. A detailed list of the critical *r* values for all potential drivers and months is provided in the Supplement (Table S8).

The r values were regionally mapped out using a colour-coded approach of five different numerical ranges. The colour code is based on absolute *r* values and not on statistical significance in order to allow comparison of effect sizes not only across countries and drivers but also with the literature. Please note that the first category (yellow, denoting $|r|$ values between 0.30−0.39), does not ensure statistical significance. It has been included in the maps since these *r* values at least contain the possibility of a relationship (marginal statistical significance with $p \approx 0.10$) and could thus be interesting for further research. For the same reason, the maps not only show the maximum absolute $|r|$ for each country, each month and each driver, as specified above, but also separately the most positive (left side) and the most negative r (right side). The resulting 144 maps (Figs. S1-S6, example in Fig. 2) are grouped into 24 panels that consist of 6 maps each, allowing direct visual comparison of best positive and negative *r* values for a given potential rainfall driver (e.g. NAO) within a season. The maps also contain lag information for the best correlations.

Key regional correlation patterns of at least moderate effect size ($|r| \geq 0.40$) were captured in simplified form on results maps that inventorize the most important relationships between rainfall and potential drivers in a differentiated manner for all 12 months (Fig. 3). Countries with $|r|$ values of 0.50 or better (large effect size) were shaded in the colour of their respective potential driver (NAO blue, AMO green, IOD orange, ENSO red, PDO purple, solar activity yellow/black). The phase relationship with rainfall is indicated as a polarity sign, e.g. NAO+ or NAO-, meaning positive or negative correlation with rainfall, respectively. Comparative time series are shown in Figs. 4 and S7−18.

In addition, some second-order relationships were explored through cross wavelets. One example for each potential driver is depicted in Fig. 5. Wavelet transforms time series into time frequency space and can therefore find localized intermittent periodicities (Grinsted et al., 2004). A colour code is generated that highlights not only the best agreement (=correlation) of the oscillating pattern of the rainfall and the driver but also the main frequencies of this common oscillation which can be variable along the years 1901–2017. The relative phase relationship is shown as arrows (with same-phase pointing right, anti-phase pointing left). From such intermittently synchronous and significant frequencies, conclusions might be drawn about a possible common cause modulating the correlation between potential driver and rain.

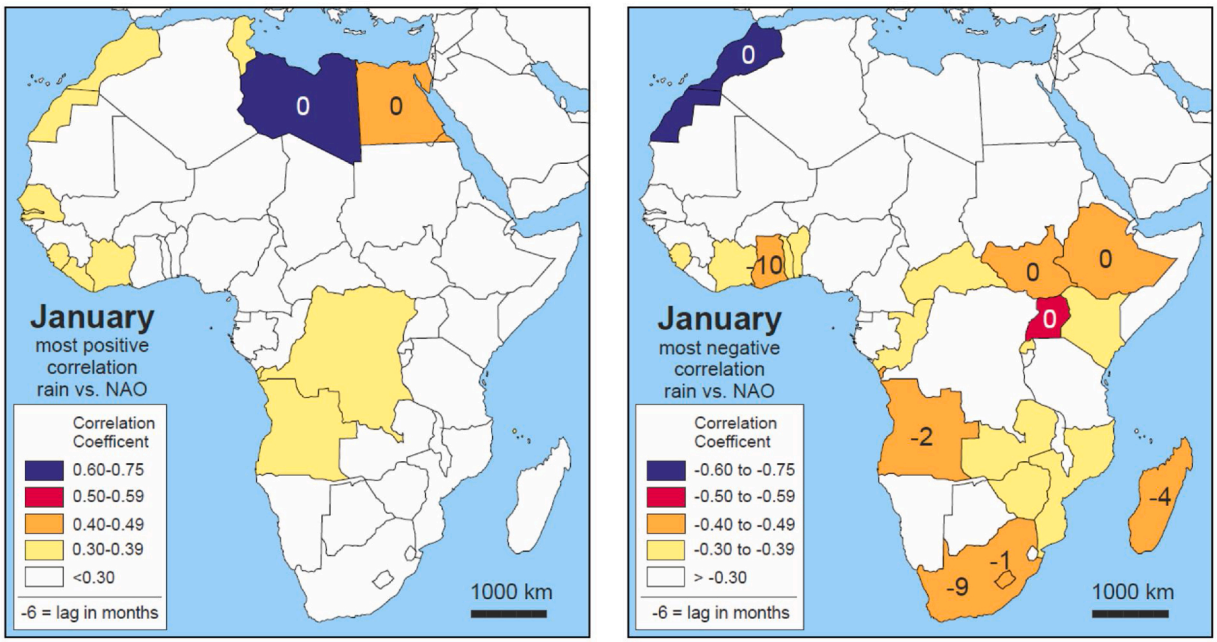

Fig. 2. Most positive (left column) and most negative (right column) correlation coefficients for January rainfall (1901-2017) of 49 African countries compared to NAO. Pearson r values and lags (in months) are from Supplement Table S2. Maps for all other months and potential climate drivers are illustrated in Supplement Figures S1-S6. Note that the yellow colour only indicates a possible effect of the potential driver since the associated r-values are only marginally statistically reliable.

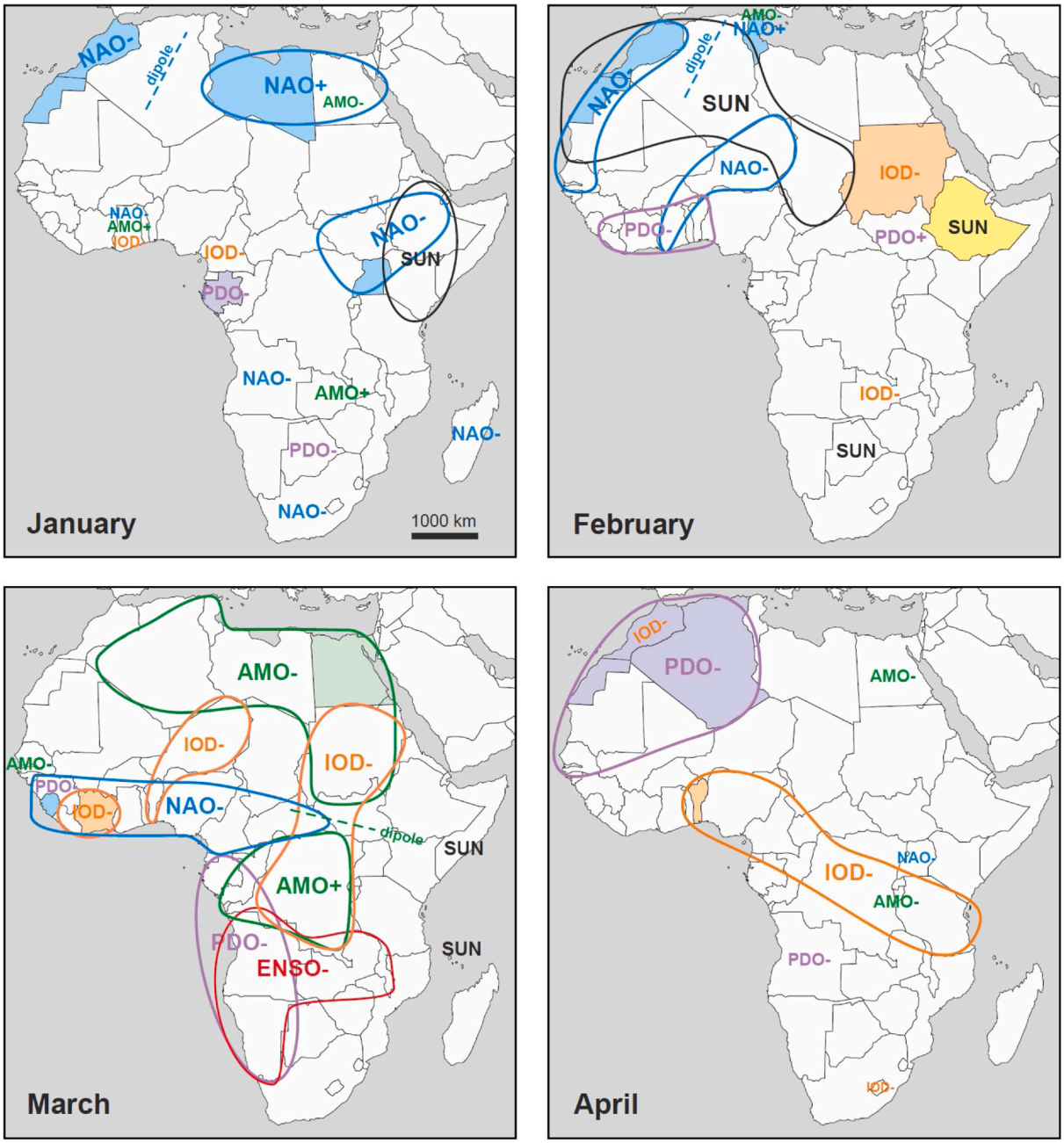

Fig. 3. Monthly maps showing regions in which rainfall correlates with oceanic modes of variability or with solar activity changes for r values ≥ 0.40 and ≤ -0.40. Positive and negative correlations with rainfall are shown (e.g. NAO+ and NAO-). Shading highlights countries in which correlations are particularly good (≥ 0.50 and ≤ -0.50). Modes of variability and solar activity changes are colour-coded: NAO = blue, AMO = green, IOD = orange, ENSO = red, PDO = purple, solar activity = black outlines and yellow fill pattern. Detailed correlation maps and statistical results tables are in Figs. S1-S6 and Tabs. S2, S4, S6, S8, S10, S12.

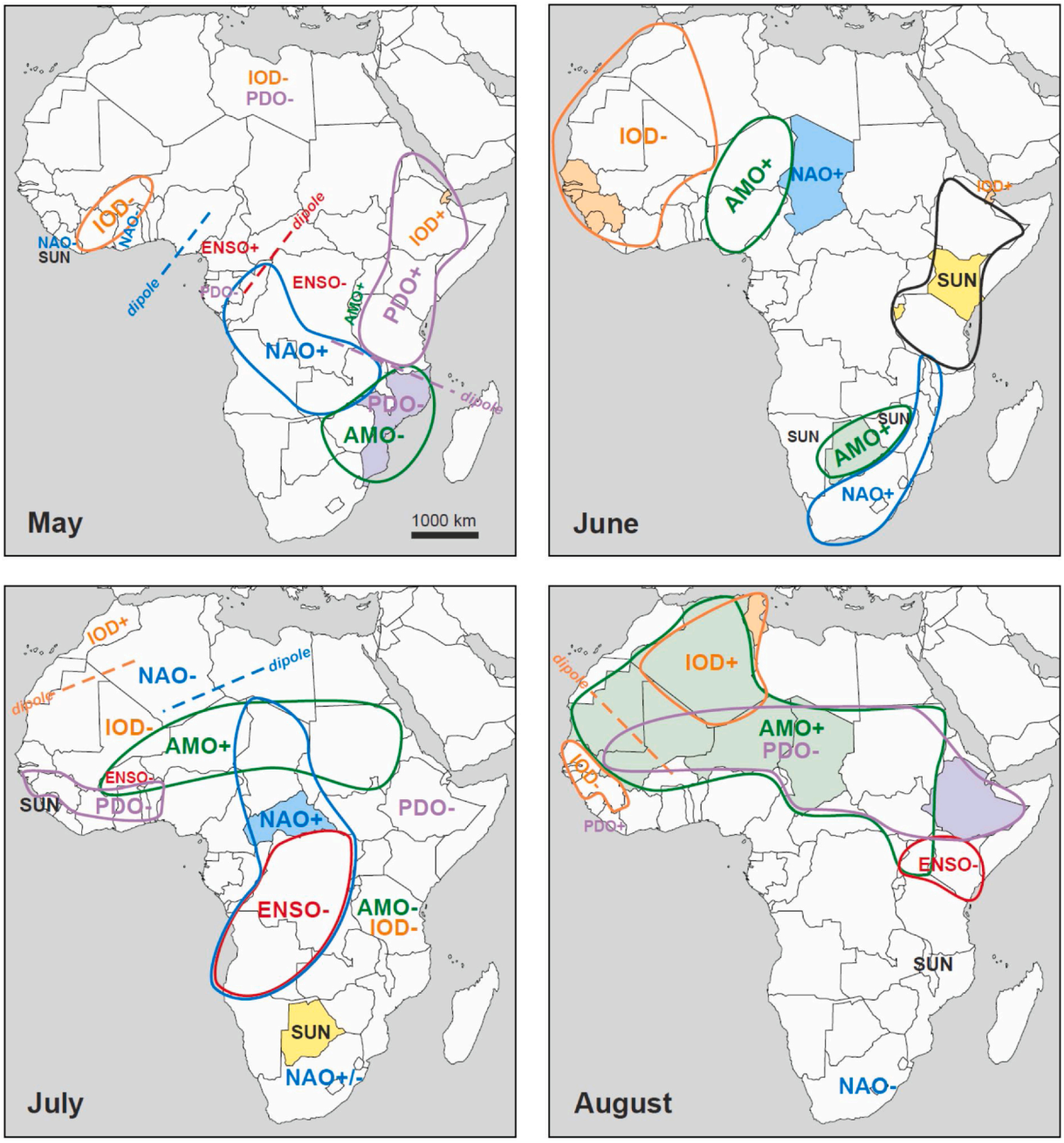

Fig. 3. (*continued*).

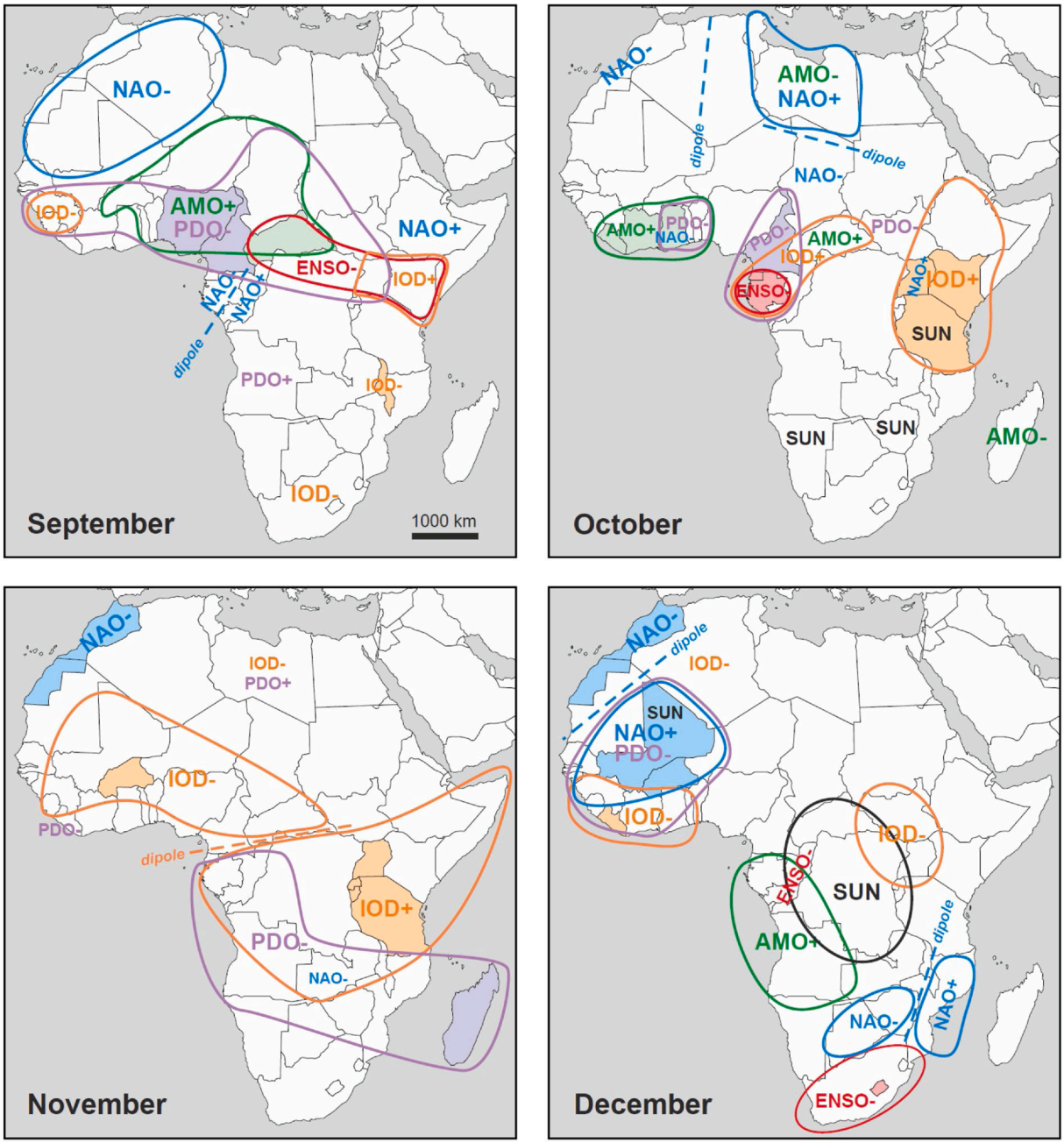

Fig. 3. (*continued*).

5. Results

In the following we are summarizing all correlations with an effect size of at least $|r| \geq 0.40$ (moderate effect) which are mostly statistically significant, although a small percentage might also be false positives due to multiple testing (see above). The results are sorted by season and respective driver. Statistical results are listed in Supplement Tables S2, S4, S6, S8, S10 and S12 which are mapped out in Supplement Figs. S1-S6. Highgraded correlations are schematically shown in Fig. 3.

5.1. *Boreal winter – austral summer (December–February)*

5.1.1. *NAO*

Rainfall in Morocco shows a strongly negative correlation with the NAO (NAO-) throughout the boreal winter season without time

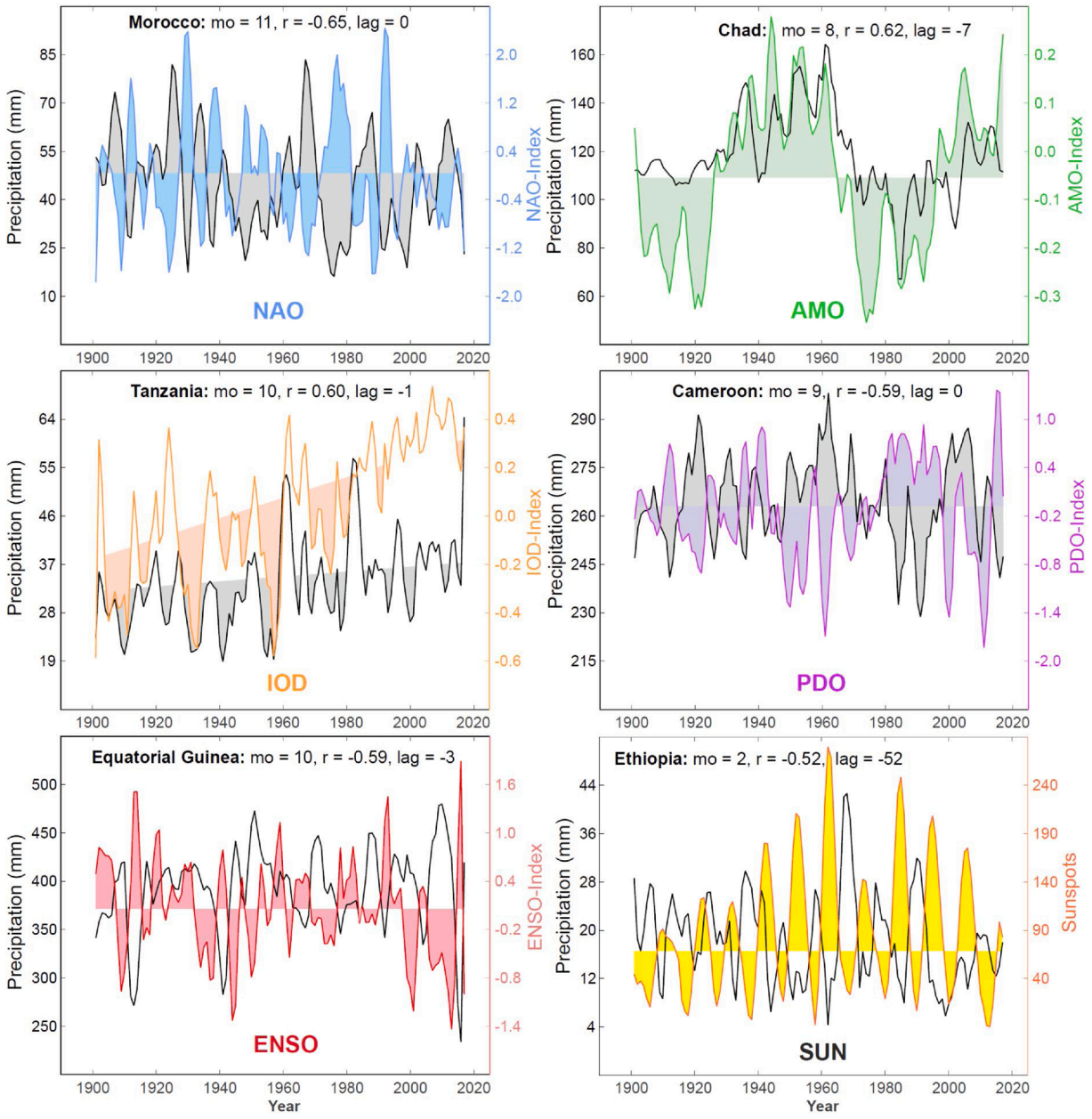

Fig. 4. Six time series illustrating the correlation of African rainfall with NAO, AMO, IOD, PDO, ENSO and solar activity changes. mo = month (January = 1, December = 12), r = Pearson correlation coefficient, lag is given in months (-1 means that potential driver precedes rainfall by 1 month). Detailed correlation maps in Figs. S1-S6, full statistical results are in tables S2, S4, S6, S8, S10, S12.

lag (Figs. 2,3, S7, S13, Table S2). Dipoles form in December with the western Sahel (Mali, Burkina Faso), in January with Libya and Egypt (Fig. 2), and in February with Tunisia, where rainfall is positively correlated with the NAO (NAO+) (Figs. 3, S7, S13). Notably, the western Sahel best positive correlations require a lag of 7 months ("lag -7") between NAO and rainfall (e.g. Guinea, Fig. S13), Tunisia has a lag of -3, whilst no lag is observed in the correlations of Libya and Egypt (Fig. S1, Tab. S2). A moderate NAO dipole occurs in southern Africa in December with NAO- correlations in Botswana/Zimbabwe (lag -9, Tab. S2, Fig. S13) and NAO+ to the east in Mozambique (lag -2) (Figs. 3, Tab. S2). The southern African NAO dipole disappears in January and is replaced by patchy NAO- correlations in Angola (lag -2), South Africa (lag -9), Madagascar (lag -4), northern East Africa (without lag, e.g. Uganda in Figs. S7, S13), and Ghana (lag -10). NAO- effects are absent in most regions in Africa in February, except for some countries in West and Northwest Africa (Ghana, lag -11; Niger, lag -8; Senegal, lag 0) (Fig. 3).

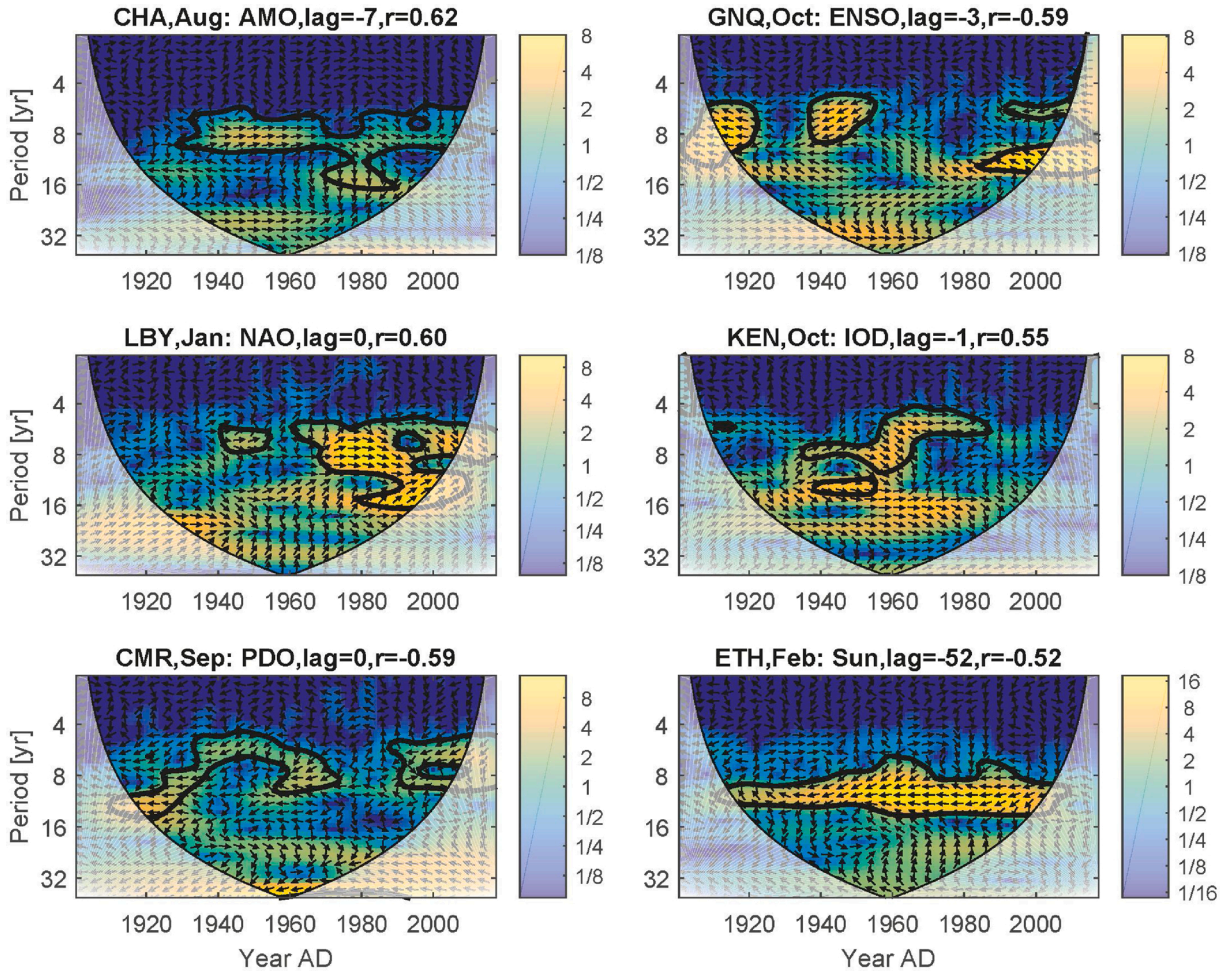

Fig. 5. Cross wavelet transforms in time-frequency space according to Grinsted et al. (2004) of six correlation examples conducted for the month and country with the strongest correlation with the respective rainfall time series: AMO (Chad August rain), ENSO (Equatorial Guinea, October rain), NAO (Libya, January rain), IOD (Kenya, October rain), PDO (Cameroon, September rain), and solar activity (Ethiopia, February rain). The power spectrum is indicated by the colour code at the right. The 5% significance level against red noise is shown as a thick contour. The relative phase relationship is shown as arrows (with in-phase pointing right, anti-phase pointing left).

5.1.2. AMO

A moderate AMO+ correlation occurs in December along the Central African Atlantic coast from Angola to Gabon (Figs. 3, S8). Only scattered local AMO rainfall effects were recorded for the subsequent two winter months, namely AMO+ in Zambia in January (lag -9), Ghana in January (lag -10), AMO- in Egypt in January (lag 0), and AMO- in Tunisia in February (lag -9) (Figs. S8, S14).

5.1.3. IOD

Various regions in Africa show strong to moderate IOD- correlations in winter, most significantly developed along the Gulf of Guinea coast (December-January, lags -2 to -8; Fig. S9) and in Sudan (February, lag -3; Figs. S9, S15). More moderate IOD- correlations in December occur in Uganda, South Sudan and Algeria in December (all with lags around -7), and in Zambia in February (lag -3).

5.1.4. PDO

Strong PDO- correlations are registered in Gabon during January (lag -6, Figs. S10, S16, Tab. S8), whilst more moderate PDO- effects influence rainfall in West Africa in December (lags 0 to -9; Fig. S10) and February (lags -9 to -11). Local PDO- correlations occur in Botswana (lag 0) in January whilst a PDO+ correlation is typically present in South Sudan in February (lag -3).

5.1.5. ENSO

Moderate ENSO- correlations occur during December in South Africa and Lesotho (both lag -6; Figs. S11, S17), as well as in Central Africa with best matches achieved in R Congo (lag -9) (Tab. S10). No major ENSO effects on African rainfall are registered in January and February.

5.1.6. SUN

December rainfall in large parts of Central Africa is moderately correlated with solar activity changes (DR Congo: r=-0.45, lag -34). Particularly good correlations are registered 1930–1995 (Figs. S12, S18). In January, a moderate correlation occurs in Ethopia and Kenya, whereby the Ethiopian correlation subsequently strengthens greatly during February (r=-0.52, lag -52). Here, excellent synchronicity between solar activity and rainfall exists for more than half a century during the period 1930–1995 (Figs. 4, S12). Interestingly, solar amplitudes are even reflected proportionally in the rainfall record when exploratively considering longer lags of up to -120 (Fig. S12). As typical for good solar correlations, the r coefficient changes polarity when the lag is increased or decreased by half of a Schwabe cycle (Fig. S21). February rain in large parts of Northwest Africa is moderately correlated with solar activity (e.g. Morocco, r=-0.41, lag -15; Fig. S12). February rain in Botswana (lag -38) shows a positive solar correlation 1900–1930 and an anticorrelation 1930–2015 (Fig. S12).

5.2. Boreal spring – austral autumn (March–May)

5.2.1. NAO

In March, Morocco loses its NAO- correlation that is so prominent in autumn and winter. The moderate NAO- correlations observed in West Africa in February further intensify in March when the entire Gulf of Guinea coastal countries and the eastward extension up to the Central African Republic are under NAO- influence. The best correlation is observed in Sierra Leone (r=-0.60, lag = 0; Figs. S7, S13). Significant negative NAO correlations are absent in Africa in April (except for NAO- in Uganda) but return to a moderate extent to some of the countries in May (Liberia, Ghana; Tab. S2). Moderate positive NAO+ correlations occur in May in a central African area reaching from R Congo to Zambia, possibly indicating some sort of NAO dipole axis in the Nigeria/Cameroon region (Figs. 3, S1, S7).

5.2.2. AMO

March rainfall in North Africa (except for Morocco) and Sudan is correlated negatively with the AMO. The best correlation is achieved in Egypt (r=-0.59, lag = 0; Fig. S8). Positive AMO correlations occur in the Congo Basin (R Congo, DR Congo; lag -2 and -1 respectively) suggesting an AMO dipole axis in South Sudan. AMO influence weakens significantly in April when only Egypt (lag 0) remains and Burundi (lag -6) newly gets under AMO- influence (Tab. S2). In May, Burundi switches to a weak AMO+ correlation, with best values registered in neighbouring Rwanda (r=+0.41, lag -4). Significant AMO- correlations now occur in southeastern Africa, mainly Zimbabwe (r=-0.49, lag -10) and Mozambique (r=-0.47, lag 0, Fig. S14).

5.2.3. IOD

Rainfall in various areas in Africa is negatively correlated with the IOD during spring. In March, the effect exists in regions stretching from the Congo Basin to Sudan, from Benin to Niger and from Cote d'Ivoire to Liberia. In April, IOD- influence occurs in a large southeast-northwest-trending belt reaching from Tanzania (lag 0) to Togo (lag -11) as well as in Lesotho and Morocco, whilst in May it exists in Cote d'Ivoire-Burkina Faso (lag -8 to -9) (Fig. S3, Tab. S6). In contrast, rainfall in Ethiopia is positively correlated with the IOD. The best correlation is achieved in nearby Djibouti (r=+0.52, lag=-10).

5.2.4. PDO

Rainfall in several African regions is linked negatively with the PDO with particularly strong correlations in Northwest Africa (April, Figs. S10, S16) and Mozambique (May). More moderate PDO- correlations occur along the Atlantic coast of central and southern Africa (March), in Guinea (March), Angola (April), Gabon (May), and Libya (May). In contrast, May rainfall in Eastern Africa is positively correlated with the PDO, forming a dipole with the negative correlations in Mozambique (Fig. S10).

5.2.5. ENSO

March rainfall in parts of southwestern Africa (Namibia, Angola, Zambia) is negatively correlated with ENSO (Figs. S11, S17). No ENSO effects are registered in April, whilst in May an ENSO dipole occurs in the central part of Africa with ENSO+ in Cameroon (Figs. S11, S17) and ENSO- in DR Congo.

5.2.6. SUN

March rainfall in Somalia shows an anticorrelation during 1910–1930 and a positive correlation during 1930–1995. In the latter interval, a lag of -120 results in a good match of relative amplitudes in both rainfall and solar activity (Fig. S12). No solar correlations with African rainfall were found during April. In May, moderate solar correlations occur in western West Africa, where correlations are mostly weak but are improving to moderate in Liberia (r=+0.40, lag -23). Good synchronicity is achieved since 1930 (Fig. S12).

5.3. Boreal summer – austral winter (June-August)

5.3.1. NAO

June is characterized by a strong NAO+ correlation in Chad (r=+0.54, lag=-9) and moderate to weak NAO+ influence on rain in southwestern Africa (South Africa to Malawi) (Figs. 3, S1, S7, S13). During July, the NAO+ region (lag -10) enlarges from Chad southwards to Angola, with the strongest correlations achieved in the Central African Republic (r = 0.57; Fig. S13). A NAO- correlation is registered in Algeria (r=-0.44, lag -1), forming a NAO dipole with Chad. During July and August a NAO- correlation in South Africa gradually turns into a NAO+ relationship. Apart from South Africa, there are no other regions with NAO influence on rainfall in

August.

5.3.2. AMO

Large parts of the Sahel zone countries are under AMO+ influence during the summer months (Fig. S2, Tab. S4). The zone of correlation is still small in June (Niger-Nigeria, lag -2) but gradually enlarges during July (belt reaching from Burkina Faso to Sudan, lags -6 to -8), leading to strongly positive correlations in August with an area comprising all Sahel countries (lags -7 to -9, Figs. 4, S8) and best r values in the central and western part (e.g. Chad, Niger with $r \geq 0.60$; Fig. S14). In June, a strong AMO+ correlation occurs in Botswana (Fig. S8), extending with more moderate r values into Zimbabwe. A moderate AMO- correlation is registered in July in Tanzania.

5.3.3. IOD

In June, all of NW Africa is influenced by IOD- (Figs. 3, S9, S15). This changes in July and August, when the northern part of the region shows IOD+ correlations (Morocco in July, Algeria and Tunisia in August; Fig. S9) whilst some countries in southern NW Africa remain negatively correlated with IOD (Mali in July, Senegal to Guinea in August; Fig. S3), establishing an IOD dipole during those months. Djibouti shows a strong IOD+ correlation in June ($r = 0.60$, lag=-6; Fig. S15), similar as already in May. IOD- influence occurs in Tanzania in July.

5.3.4. PDO

The PDO plays no role for African rainfall in June. Negative PDO correlations establish along parts of the West African Atlantic coast and in Ethiopia in July. In August, the PDO- zone enlarges across the entire Sahel except for the Atlantic coast which is now dominated by IOD- (Fig. 3). Only in Liberia August rain is positively correlated with the PDO (Fig. S16).

5.3.5. ENSO

There is no major ENSO influence on African rainfall in June (Tab. S10). Negative ENSO correlations, however, occur during the other two summer months, namely in DR Congo-Angola (Fig. S11) and Burkina Faso (both July) as well as in Kenya-Uganda (August, Figs. S11, S17).

5.3.6. SUN

Good and moderate correlations between solar activity and summer rainfall occur in various places across Africa. The best r values are registered in East Africa in June (Kenya r=-0.55, lag=-33; Burundi r=-0.52, lag -21; Fig. S18) and in Botswana in July ($r = 0.51$, lag -31) (Figs. S12, S18). Burundi shows a good anticorrelation throughout the last 120 years. In Botswana, an anticorrelation 1920–1930 switches to a good positive correlation 1930–1995 in which respective amplitudes of solar activity are reflected in the rain fall record (Fig. S12).

5.4. Boreal autumn – austral spring (September-November)

5.4.1. NAO

Rainfall in NW Africa is negatively correlated with the NAO during the boreal autumn months, similar as in winter (Figs. 3,4, S7, S13, Tab. S2). The NAO- correlation initially extends over most of NW Africa, but is reduced to Morocco during October where the linkage further intensifies in November. Several dipoles are developed during this season, namely in Gabon (NAO-) vs. R. Congo (NAO+) in September, and in Libya (NAO+) vs. Morocco and Chad (both NAO-) in October. Moderate correlations are observed in Ethiopia (NAO+ in September), Ghana (NAO- in October), Uganda (NAO+ in October), and Zambia (NAO- in November, Fig. S7).

5.4.2. AMO

Moderate to strong AMO correlations occur in both September and October (lags mostly -8 to -9), but not in November. September rain is positively correlated to AMO in a belt stretching from Burkina Faso to the Central African Republic (Figs. 3, S8; Tab. S4). This belt disintegrates in October, when AMO+ correlations are restricted to some Gulf of Guinea coastal countries and the Central African Republic. Rainfall in Libya and Madagascar (Fig. S8) is negatively correlated with the AMO in October.

5.4.3. IOD

For September, patchy negative IOD correlations are registered in Guinea/Sierra Leone, Malawi and South Africa/Lesotho (Figs. S9, S15; Tab. S6). Rainfall in Kenya and Uganda, however, is positively correlated with the IOD. The East African IOD+ correlation further expands and intensifies in October when strong correlations occur in Tanzania (Fig. S4), Kenya and Uganda (Fig. S15). The zone of IOD+ influence reaches up to Ethiopia where moderate r values are seen (lags 0 to -3). Another region with IOD+ correlations in October occurs in a belt reaching from Gabon to the Central African Republic (lag -8) (Fig. S3). A large-scale IOD dipole is developed in Africa in November. The majority of West Africa is under IOD- influence, whilst rain in Central and East Africa are positively correlated with the IOD (Figs. 3, S15).

5.4.4. PDO

Rainfall is negatively correlated with the PDO in large parts of Africa during boreal autumn / austral spring. In September, this belt covers most of West Africa and reaches eastwards into Uganda. Best PDO- correlations occur in Nigeria, Cameroon ($r = -0.59$, Figs. 4,

S16), and the Central African Republic (all with lag 0). The belt disintegrates in October when such correlations are restricted to Ghana-Togo-Benin, Equatorial Guinea-Gabon-Cameroon (Fig. S10) and South Sudan. In November, the PDO- belt moves south and covers a wide swath from Gabon to Madagascar across the northern part of southern Africa (Figs. 3, S10, S16; Tab. S8).

5.4.5. ENSO

ENSO influence on African rainfall is restricted to two regions during this season. In September, moderate ENSO- correlations occur in a belt from the Central African Republic to Kenya. Strongly negative correlations of rainfall with ENSO were registered for October in Gabon (Fig. S17) and Equatorial Guinea (Figs. 4, S11, S17). All lags are small (0 to -3).

5.4.6. SUN

Solar activity shows moderate correlations with austral spring rainfall in several southern and eastern African countries. September rainfall in Namibia shows a good positive correlation with solar activity during the interval 1955–1985 when even relative amplitudes of both parameters match (lag -105; Fig. S12). The sun keeps influencing rainfall in Namibia in the subsequent month of October with particularly good synchronicity 1930–1995 (lag -53) (Fig. S12). Other countries with a solar signal in their rainfall are Eritrea (October, good negative correlation 1960–2005, lag -46), Zimbabwe (October, good correlation 1930–1985, lag -12), and South Africa (November, good correlation 1950–1980, lag -66) (Fig. S12).

The exploratory cross-wavelet transform for the SUN shows that over the entire time series there is significant common power in the frequency band corresponding to a period of about 10–12 years, which is the length of the Schwabe cycle (Fig. 5). For every other potential driver NAO, AMO, IOD, PDO and ENSO, there is also significant common power in this frequency range, however not continuously but intermittently. For example, the IOD correlation between October rain in Kenia (middle right panel) computed across the entire time series was $r = 0.55$ (lag -1). However, the wavelet transform reveals that in the time window between 1940–1980 both time series oscillate with a common period of roughly 8 years, whereas between 1940–1960 there is a second significant frequency band corresponding to a period of about 14 years. Similar patterns were obtained for the other potential drivers.

6. Discussion

The lag-optimized correlation analysis demonstrates that African rainfall is correlated with a diverse set of potential drivers characterized by a clear seasonal month-by-month evolution and complex lag relationships. In the following we are discussing some of the key correlation patterns that were identified in our lag-optimizing cross correlation analysis, and compare them to previously reported findings.

6.1. NAO

We confirmed that boreal autumn and winter rainfall in Morocco is strongly negatively correlated with the NAO (Fig. 3), because a negative NAO diverts the moisture-laden westerly winds southwards to Iberia and northwest Africa (Knippertz et al., 2003a). The effect fades away in March, as also confirmed by Marchane et al. (2016), because the phase relationship between NAO and rainfall becomes more unstable over time. Whilst March is still dominated by a weak negative correlation (r=-0.38, lag 0), April rain in Morocco shows multidecadal intervals with both negative and positive NAO correlations (Knippertz et al., 2003b; Turki et al., 2016) (Fig. S7). The non-stationary relationship with repeated phase reversals results in an apparent overall non-correlation of April rain, when considering the last 117 years.

We further found positive NAO correlations in central and eastern North Africa, namely Tunisia/Libya (October), Libya/Egypt (January) and Tunisia (February) (Fig. 3). This North African west-east NAO rainfall dipole matches with previous analyses of modern precipitation data (Brandimarte et al., 2011; López-Moreno et al., 2011), and is also known from palaeoclimatic studies covering multicentennial timescales (Nieto-Moreno et al., 2015; Roberts et al., 2012; Sánchez-López et al., 2016). The dipole axis is located within Algeria, whereby winter rainfall in northwestern Algeria is still negatively correlated with NAO, whereas the northeastern part of the country does not show systematic NAO influence (Taibi et al., 2017).

Linderholm et al. (2009) suggested a negative NAO correlation of Sahel rainfall in July and August, which however we could not fully replicate in our analysis, possibly due to mismatches in Sahel rainfall datasets (Berntell et al., 2018). An exception is Algerian rainfall in July, which is dominated by the Sahel rain in southernmost Algeria. Here we found a negative NAO correlation, in line with the findings of Linderholm et al. (2009).

A strongly positive NAO correlation occurs in June in Chad. In the subsequent month of July the correlation weakens a bit in Chad but expands greatly southward to form a 4000 km long belt reaching to Angola, with a particulary well developed NAO+ correlation in the Central African Republic (Fig. 3). A strong NAO+ correlation also occurs in December in Mali and Burkina Faso, forming a dipole with a pronounced NAO- correlation in Morocco (Fig. 3).

During March, rainfall in a 4000 km long west-east belt stretching from Guinea to the Central African Republic correlates negatively with the NAO. This partly matches with the findings of Li et al. (2012) who suggested that the West African summer monsoon is negatively correlated with boreal spring NAO. However, we identified a more direct linkage of March NAO with March rain, without involving major time lags (Fig. 3, S7, Table S2). The reason for the discrepancy may be the shorter time interval studied by Li et al. (2012), i.e. 1979–2010 vs. our time interval of 1901–2017, potentially involving non-stationary correlation effects.

The strongest apparent influence of NAO on East African rainfall occurs in January when a negative correlation is registered over the entire northern part of the region. A similar relation was already previously reported by McHugh and Rogers (2001) and Mpelasoka

et al. (2018). Uganda shows the greatest r values for January in our analysis, with a more moderate correlation for the long rains in April (Fig. S7). In contrast, some of the boreal autumn rains in the region correlate positively with NAO, as evidenced in Ethiopia (September) and Uganda (October), highlighting the need for detailed seasonal differentiation in rainfall and drought analyses. This is also further illustrated by the austral winter rain in South Africa that is initially correlated positively with NAO in June, but changes into a negative correlation by August (Fig. S1). Further differentiation of South African rainfall trends on a province-level would be necessary to better understand regional details.

6.2. AMO

Among the most prominent and best studied relationships is the positive AMO correlation with summer Sahel rain (e.g. Folland et al., 1986; O'Reilly et al., 2017; Shanahan et al., 2009; Zhang et al., 2019) which our analysis fully agrees with. The correlation slowly begins to form in June, expands over the entire Sahel in July and peaks in intensity in August (Fig. 3). It still covers a large area in September, although less intense, and begins to regionally disintegrate in October (Fig. 3). The best positive correlation of AMO and Sahel rainfall has a time lag of about 7 months (Fig. S2). Comparison of rain and AMO without lag (instantaneous correlation) yields significantly poorer correlations. In addition, non-stationary effects occur, as correlations in the first half of the 20th century were partly negative or absent (Diatta and Fink, 2014) (Fig. S8). Notably, a variety of different Sahel rain datasets exist which partly conflict with each other (Berntell et al., 2018). Many simulation studies still fail to fully replicate the scale of the relationship between Sahel rain and AMO (Knight et al., 2006; Martin et al., 2014).

Some authors have reported an equatorial belt to the south of the Sahel with regions of summer/autumn negative AMO correlations (Diem et al., 2014; O'Reilly et al., 2017; Ogou et al., 2019; Zhang and Delworth, 2006; Zhang et al., 2019), which could not be detected by our analysis, possibly due to weaker correlation intensities and limited areal extent. It may also be a result of non-stationary correlations. According to Losada et al. (2012) an anti-correlation between rainfall anomalies in the Sahel and the Gulf of Guinea coast existed before the 1970's forming a dipole (negative AMO correlation e.g. in Equatorial Guinea in August, Fig. S2). However, the dipole pattern almost disappeared after that date (Losada et al., 2012).

Our study identified positive AMO correlations in Central Africa during two months, namely in the greater Congo Basin in March and along the Atlantic coast from Gabon to Angola in December (Fig. 3). October rainfall in Madagascar is characterized by a negative AMO correlation. Similar correlations were already reported by Martin and Thorncroft (2014). Taye and Willems (2012) reported a strong positive correlation in the Ethiopian Blue Nile basin of October-February rainfall with AMO. We could not detect this correlation in our study probably because the Blue Nile basin is located in the northwestern part of the country and rainfall in other parts of Ethiopia may have different relationships with AMO. Based on countrywide data, we only found a weakly positive AMO correlation in December (Fig. S2). The importance of high-resolution seasonal differentiation is underlined by the rainfall anomalies in Zimbabwe. Whilst rain is negatively correlated with AMO in May, the correlation turns positive in June. The AMO- area in May extends eastwards into Mozambique, the AMO+ area in June extends westwards, with a strongly positive AMO correlation in Botswana (Fig. S8). Our results newly suggest AMO relationships in March, characterized by a negative correlation in North Africa and Sudan, and a positive one in the Congo basin, resulting in a dipole axis in South Sudan.

6.3. IOD

The IOD plays a major role for African rainfall during most months of the year. The best known and most pronounced influence occurs during the short rain season in East Africa in September to November when rainfall is strongly positively correlated to the IOD (e.g. Black, 2005; Marchant et al., 2007; Saji et al., 1999). In our analysis the effect initially appears in Kenya-Uganda in September with moderate correlation strength, and subsequently intensifies and expands north- and southwards in October. By November, most of East and Central Africa are positively correlated with IOD (Bahaga et al., 2015; Behera et al., 2005), with a strong core area along the Uganda-Tanzania axis (Fig. 3). During that month a major IOD rainfall dipole forms with West Africa which is negatively correlated with the IOD (Bahaga et al., 2015; Diatta and Fink, 2014). The typical IOD+ correlation occasionally flips to IOD- as seen in an October time series for Tanzania where such inversions occurred in the 1920s and 1980s (Clark et al., 2003; Owiti et al., 2008) (Fig. S9). The effect could be due to an interference with the solar activity signal that in the same country and month shows significant correlation with rainfall (r=+0.40, lag -34) (Figs. 3, S6). Also other authors report non-stationary IOD correlations of various kinds with the East African short rains (Manatsa and Behera, 2013).

Strong and/or widespread negative IOD correlations also occur in Sudan in February, in March and April in various places in the interior of Africa, in June in large parts of West and Northwest Africa (Diatta and Fink, 2014), and in December along the Gulf of Guinea coast (Fig. 3). IOD rainfall dipoles occur in Northwest and West Africa during July and August (Bahaga et al., 2015; Behera et al., 2003) (Fig. 3). In South Africa, the only month with IOD influence is September when rainfall shows an overall moderate negative correlation with IOD (Behera et al., 2003), although the correlation is very much non-stationary when inspecting the time series in detail (Fig. S9) (Manatsa et al., 2012). In the same month, an IOD- correlation also occurs in Malawi, forming a potential dipole with the IOD + correlation observed in northern East Africa (Bahaga et al., 2015; Zhang et al., 2015) (Fig. 3). Rainfall in southern Africa during January and February does not yield any moderate or strong correlations with IOD over the past 115 years. However, visual analysis of the January and February time series of South Africa and Lesotho show that positive and negative correlations alternated on a decadal to multi-decadal basis (Fig. S9), highlighting significant non-stationary IOD relationships (Manatsa et al., 2012), most likely as a response to ENSO interaction (Manatsa and Mukwada, 2012). Cross wavelet analyses as explored in Fig. 5 could capture this effect.

6.4. PDO

The PDO correlates with African rainfall somewhere on the continent in all months of the year, except in June. In most cases rainfall is negatively correlated with the PDO. During the period July-October, rainfall in the Sahel and sub-Saharan northern equatorial belt is correlated to both AMO and PDO, whereby their respective regions of correlation are partly overlapping or adjacent to each other (Diatta and Fink, 2014; Mohino et al., 2011; Mpelasoka et al., 2018; Ogou et al., 2019; Taye and Willems, 2012) (Fig. 3). Negative PDO correlations occur in western Central Africa repeatedly over the year, namely in January, March, October and November, whilst they are recorded in Northwest Africa during April and December (Fig. 3). Positive PDO correlations exist only in East Africa in February and May. During May, a dipole forms with Mozambique where rainfall is strongly negatively correlated with the PDO. In November the negative IOD correlation extends from Gabon across the entire continent to Madagascar where the relation is the strongest.

6.5. ENSO

We found negative ENSO correlations with African rainfall occurring in March (Southwest Africa), May (Congo Basin), July (Central Africa), August and September (northern East Africa), October (Gabon, Equatorial Guinea) and December (South Africa, Lesotho and R. Congo). The only significant positive ENSO correlation is recorded in May in Cameroon which forms a dipole with the negative ENSO correlation in DR Congo (Fig. 3). The ENSO relationship to seasonal East African rainfall is a well-known general feature (e.g. Fer et al., 2017; Funk et al., 2018; Hoell et al., 2014; Indeje et al., 2000; Kiladis and Diaz, 1989; Ropelewski and Halpert, 1987; Williams and Funk, 2011).

Nevertheless, the occasional link-up of droughts and La Niña conditions in parts of East Africa (i.e. a positive ENSO correlation) (Lott et al., 2013; Lyon and DeWitt, 2012) was not detected in our study as a longterm anomaly over the past 117 years of data. The reason may be because the ENSO correlation of the East African short rains in September-November is highly time-dependent over the past 140 years with an alternation of multidecadal intervals of good and poor correlations (Clark et al., 2003; Nicholson, 2015). Furthermore, rainfall modulation in the region is believed to be dependent on both ENSO and IOD (Black et al., 2003; Hoell and Funk, 2014; Mpelasoka et al., 2018), and the IOD signal appears in our study very prominently in the East African short rain season, overshadowing the ENSO contribution (Fig. 3).

A negative ENSO correlation with summer rainfall in Ethiopia has been widely reported (e.g. Korecha and Barnston, 2007; Zaroug et al., 2014) but only weakly negative correlations in August were found in our study (Fig. S5, Table S10). This is most probably because the easternmost part of Ethiopia is known to correlate positively with ENSO (e.g. Funk, 2011; Korecha and Barnston, 2007), resulting in a heterogeneous overall ENSO response in Ethiopia on a country-wide scale (Korecha and Barnston, 2007). We did neither detect significant ENSO correlations with rainfall in West Africa nor the Sahel (Biasutti, 2019), except for July rain in Burkina Faso which shows a moderate negative correlation.

In contrast, rainfall in Central Africa is primarily negatively correlated to ENSO during several months of the year. As a consequence, discharge of the Congo River is also negatively correlated with ENSO (Amarasekera et al., 1997). An ENSO dipole occurs in May with a positive ENSO correlation in Cameroon and a negative correlation in DR Congo (Fig. 3). The complexity of arguments for ENSO influence on rainfall in the region was already pointed out by Balas et al. (2007) and Dezfuli and Nicholson (2013).

Negative ENSO correlations in March of Angola and Zambia are associated with a rainfall lag of 5 months, and the correlations in July of Angola and DR Congo with lags of 10 and 6 months, respectively (Fig. S5, Table S10). There is no instantaneous response of rainfall to ENSO in these regions and months. We have also explored longer lag times of up to 36 months. The only case in which this resulted in a significant improvement was June rainfall of Equatorial Guinea which shows a moderate negative correlation with ENSO with a lag of -27, whilst lags up to 11 months did not yield a convincing relationship.

We confirmed earlier results that austral summer rainfall in southern Africa is negatively correlated with ENSO (Funk et al., 2018; Hoell et al., 2015, 2017; Kane, 2009; Mason and Goddard, 2001). December rainfall in South Africa is moderately negatively correlated with ENSO and rain in Lesotho even strongly negatively correlated (Fig. 3). The choice of longer lags of up to 36 months does not bring further improvement for ENSO correlation indices, except for the Comoros in March ($r = -0.40$ with lag -36, no correlation with shorter lags up to 11 months).

Several authors have reported negative ENSO correlations with rainfall in Morocco, northwest Algeria and Tunisia (Knippertz et al., 2003b; Meddi et al., 2010; Ouachani et al., 2013; Rodó et al., 1997; Zeroual et al., 2016). We did not detect any significant ENSO correlation within the chosen 11 months lag time window (Fig. S5). Inspired by Ouachani et al. (2013) who reported time lags of 2 years between ENSO signal and rain in Northwest Africa, we have experimented with lag times of up to 36 months. This indeed produced moderate negative correlations, although just for the dry boreal summer month of August with insignificant total rainfall (e.g. Morocco -0.44, lag -35; Algeria -0.40, lag -33; Tunisia -0.41, lag -21). Also other studies struggled to document significant ENSO correlations in Northwest Africa (e.g. Bougara et al., 2020), most likely because the coupling between ENSO and rain has repeatedly weakened over a few decades (Knippertz et al., 2003b). Clearly, the key driver of winter rainfall in the region is the NAO, whilst IOD plays a role for rainfall during the summer months (Fig. 3).

6.6. SUN

In agreement with previous studies highlighting a solar influence on African rainfall (e.g. Ait Brahim et al., 2018; Alexander et al., 2007; Gachari et al., 2014; van Loon et al., 2004), we identified moderate to strong solar correlations with rainfall in at least some locations in many months of the year, except during April, September and November (Fig. 3). The strongest solar correlations occur in

Ethiopia in February, in Kenya and Burundi in June, and in Botswana in July. These are all low rainfall months, suggesting that strong solar influence in these cases controls rare rain showers in the dry season. Cross wavelets for February rain in Ethiopia correspondingly show a distinct 11 year cyclicity across the entire time series (Fig. 5).

More moderate solar correlations were also found in the high rainfall season, namely for a large area in Northwest Africa in February and in Botswana in February (Fig. 3). In some months the solar correlations are regionally overlapping or adjacent to NAO correlations, e.g. in East Africa in January, or in Northwest Africa in February (Fig. 3). In our study we allowed lags up to 66 months (in explorative time series plots up to 120 months) in order to account for the sinusoidal nature of the 11 year solar Schwabe cycle, non-trivial phase relationships, and delayed solar-forced rainfall response. The identified solar correlations are characterized by a diverse range of lags, reflecting multi-year response delays and/or complex phase relationships. In some cases, relative amplitudes of solar signal and rainfall anomaly match best, when considering long lags of ~9 years (e.g. Ethiopia in February, Namibia in September) (Figs. S12). Very rarely, optimal solar correlations involve zero lag relationships, e.g. in the Central African Republic in December (Fig. S6). In some cases there are both significant positive and negative solar correlations for lags shifted by a half cycle (e.g. DR Congo in December, East Africa in June, Namibia in October) (Fig. S21) due to the nearly sinusoidal nature of the solar Schwabe cycle.

As stated in the theoretical section 3.6 and backed up with comprehensive literature, solar activity influences most oceanic modes of variability and is therefore likely to contribute indirectly in a non-linear way to changes in African rainfall. Our exemplary and explorative cross wavelet analysis in Fig. 5 supports this notion: In every potential oceanic driver, a temporally intermittent common oscillatory period of roughly 10–12 years between oceanic driver and rainfall is seen. It suggests that a physical cause oscillating with the common significant period might intermittently influence the oceanic oscillation, which in turn drives the rainfall. Since in all six pictures, the intermittently significant common power has a period of roughly about 10–12 years, part of the cause might be the sun. However, more research is needed on this topic.

6.7. *Mid-term forecasting potential*

Based on the empirical relationships mapped out in this contribution and reported in the literature, rainfall prognoses in Africa can be attempted based on three main pillars. Firstly, a large number of established correlations involve a delayed rainfall response with regards to their potential drivers. This offers forecasting potential with an advance notice of the respective time lag, once the value of the potential driver has been measured.

Secondly, several modes of climate variability are now being forecast one month to more than a year ahead, e.g. ENSO (He et al., 2019; Petersik and Dijkstra, 2020), NAO (Dunstone et al., 2016; Scaife et al., 2014; Smith et al., 2016; Wang et al., 2017b), and IOD (Lim and Hendon, 2017). These forecasts allow rainfall prognoses also for relationships in which potential drivers and rainfall are instantaneously coupled, without time lags.

Thirdly, rainfall prognoses are possible based on quasi-cyclical potential drivers such as the ~60 year periods of AMO (Kerr, 2000; Ting et al., 2014) and PDO (e.g. Easterbrook, 2016) as well as the 11 year cyclicity of the solar Schwabe cycle (e.g. Hamid and Marzouk, 2018; Hathaway and Upton, 2016). This group of forecasts involves time horizons of several years or in the case of AMO and PDO even of a few decades, although only with coarser, multi-year resolution. The expected decline of the AMO in the coming years (Hermanson et al., 2014; Keenlyside et al., 2008; Klöwer et al., 2014; Sutton and Dong, 2012) will most likely reduce the amount of rainfall in the Sahel, similar as in the 1960s-80 s (Berntell et al., 2018; Zhang and Delworth, 2006). However, correlations can be non-stationary. It is therefore always necessary to verify on time series or in shorter-term Pearson correlations that the established long-term relationship is currently valid, or whether the correlation has recently flipped or failed. Due to these variations, empirically-driven rainfall prognoses can be made with a certain probability, but never with full certainty.

Explaining and forecasting are two different aims in research (Toulmin, 1961). In contrast to the attempt to establish structural relationships, as in the present research, for forecasting monthly rainfall the unsmoothed time series of both precipitation and potential driver should be used. As an example, Fig. S19 shows that even if the unsmoothed data do not fully capture the amplitude of precipitation, resulting in lower r-values, they mimic the variability from year to year with astonishing accuracy.

6.8. *Limitations and outlook*

Correlation coefficients presented here refer to the period 1901–2017, therefore averaging over a more than a century long time span during which phase relationships between rainfall and the potential driver may have changed. In cases of non-stationary correlations, the Pearson r values depend on the chosen time period. Furthermore, some correlations can only be detected when time lags are taken into consideration. More sophisticated statistical methods like cross wavelets, multiple linear regression including lag-optimization, or path analysis will be necessary in order to detect second-order relationships. In our approach we have chosen to smooth the data in order to better detect decadal and multidecadal trends. The detection of higher frequency, interannual variability requires the use of unfiltered data for which we provide statistical results in Supplement Tables S1, S3, S5, S7, S9, S11 and S20.

7. Conclusions

- African rainfall shows significant year-to-year natural fluctuations that in part are linked to teleconnections associated with modes of variability in the Atlantic, Pacific and Indian oceans. Several of these relations have already been documented in the literature, e.g. the link between the AMO and Sahel rains, the connection between the NAO and Moroccan precipitation, as well as the influence

of the IOD on the short rain season in East Africa. The present paper provides the first continent-wide analysis of the influence of six potential climatic drivers of natural variability, namely AMO, NAO, IOD, PDO, ENSO, and solar activity changes on African rainfall.

- On a month-by-month basis, we calculated Pearson *r* values for smoothed monthly rainfall data of 49 African countries over the period 1901–2017 with the six potential climatic drivers. In the search for the best correlations we allowed time lags of up to 11 months for each potential driver (66 months for solar activity). The lag-optimized Pearson coefficients were regionally mapped out across Africa separately for each of the 12 months of the year.
- For each of the five oceanic climate drivers, we found specific temporal and geographical patterns of influence on rainfall variability. The monthly approach was particularly suited to capture the dynamic of this influence over the year.
- We showed further that solar activity influences rainfall in a linear way in smaller-scale regions during certain seasons with extraordinary strength. An explorative wavelet analysis revealed that the solar Schwabe cycle left its imprint in the spectra of all five ocean cycles. This points to second-order relationships that require further research.
- Whilst our study is based on statistical correlations, we do not interpret our *r* values as indicators of direct causal physical effects. Future investigations will have to thoroughly analyze the meteorological processes behind the correlations in order to physically validate these teleconnections and integrate and replicate them in climate models.
- Our empirical results may help to further improve short- to midterm rainfall prognoses in Africa and provide important calibration data for the continuous improvement of climate models. A better understanding of African rainfall variability and potential natural drivers would help to better prepare African societies for anticipated droughts and floods by taking early precautionary action.

CRediT authorship contribution statement

Horst-Joachim Lüdecke: Methodology, Formal analysis, Investigation, Writing - review & editing, Data curation. **Gisela Müller-Plath:** Methodology, Formal analysis, Investigation, Writing - review & editing. **Michael G. Wallace:** Formal analysis, Investigation, Writing - review & editing, Validation. **Sebastian Lüning:** Writing - original draft, Project administration, Funding acquisition, Visualization.

Declaration of Competing Interest

The authors report no declarations of interest.

Acknowledgements

We thank Chris Folland for valuable discussions. Note that this study is fully unrelated to the last author's employment in the hydrocarbon sector and was neither commissioned nor funded by the energy industry. SL undertook this study outside office hours as a private person, trained geoscientist, and former full-time academic. The vectorised Africa base map in this paper was sourced from www.d-maps.com, a useful service for which we are thankful. We are grateful to three anonymous reviewers who greatly helped to improve this manuscript. We thank Jens Kröger for funding the Open Access Publication Fee.

Appendix A. Supplementary data

Supplementary material related to this article can be found, in the online version, at doi:https://doi.org/10.1016/j.ejrh.2021.100795.

References

Abtew, W., Melesse, A.M., Dessalegne, T., 2009. El Niño Southern Oscillation link to the Blue Nile River basin hydrology. Hydrol. Processes 23 (26), 3653–3660. https://doi.org/10.1002/hyp.7367.

Ait Brahim, Y., et al., 2018. Multi-decadal to centennial hydro-climate variability and linkage to solar forcing in the Western Mediterranean during the last 1000 years. Sci. Rep. 8 (1), 17446 https://doi.org/10.1038/s41598-018-35498-x.

Alexander, W.J.R., 2005. Linkages between solar activity and climatic responses. Energy Environ. 16 (2), 239–253. https://doi.org/10.1260/0958305053749462.

Alexander, W.J.R., Bailey, F., Bredenkamp, D.B., van der Merwe, A., Willemse, N., 2007. Linkages between solar activity, climate predictability and water resource development. J. South Afr. Inst. Civil Eng. 49 (2), 32–44.

Amarasekera, K.N., Lee, R.F., Williams, E.R., Eltahir, E.A.B., 1997. ENSO and the natural variability in the flow of tropical rivers. J. Hydrol. 200 (1), 24–39. https://doi.org/10.1016/S0022-1694(96)03340-9.

Badou, D.F., Kapangaziwiri, E., Diekkrüger, B., Hounkpè, J., Afouda, A., 2017. Evaluation of recent hydro-climatic changes in four tributaries of the Niger River Basin (West Africa). Hydrol. Sci. J. 62 (5), 715–728. https://doi.org/10.1080/02626667.2016.1250898.

Bahaga, T.K., Mengistu Tsidu, G., Kucharski, F., Diro, G.T., 2015. Potential predictability of the sea-surface temperature forced equatorial East African short rains interannual variability in the 20th century. Q. J. R. Meteorolog. Soc. 141 (686), 16–26. https://doi.org/10.1002/qj.2338.

Balas, N., Nicholson, S.E., Klotter, D., 2007. The relationship of rainfall variability in West Central Africa to sea-surface temperature fluctuations. Int. J. Climatol. 27 (10), 1335–1349. https://doi.org/10.1002/joc.1456.

Behera, S., et al., 2003. Impact of the Indian Ocean Dipole on the East African short rains: a CGCM study. CLIVAR Exchanges – Sci. Contrib. 27, 1–4.

Behera, S.K., et al., 2005. Paramount impact of the Indian Ocean Dipole on the East African short rains: a CGCM study. J. Clim. 18 (21), 4514–4530. https://doi.org/10.1175/jcli3541.1.

Berntell, E., Zhang, Q., Chafik, L., Körnich, H., 2018. Representation of multidecadal Sahel rainfall variability in 20th century reanalyses. Sci. Rep. 8 (1), 10937 https://doi.org/10.1038/s41598-018-29217-9.
Biasutti, M., 2019. Rainfall trends in the African Sahel: characteristics, processes, and causes. WIREs Clim. Change 10 (4), e591. https://doi.org/10.1002/wcc.591.
Black, E., 2005. The relationship between Indian Ocean sea-surface temperature and East African rainfall. Philos. Trans. R. Soc. A: Math. Phys. Eng. Sci. 363 (1826), 43–47. https://doi.org/10.1098/rsta.2004.1474. DOI.
Black, E., Slingo, J., Sperber, K.R., 2003. An observational study of the relationship between excessively strong short rains in coastal East Africa and Indian Ocean SST. Mon. Weather Rev. 131 (1), 74–94. https://doi.org/10.1175/1520-0493(2003)131<0074:aosotr>2.0.co;2.
Bougara, H., Hamed, K.B., Borgemeister, C., Tischbein, B., Kumar, N., 2020. Analyzing trend and variability of rainfall in the Tafna basin (Northwestern Algeria). Atmosphere 11 (4), 347.
Brandimarte, L., Di Baldassarre, G., Bruni, G., D'Odorico, P., Montanari, A., 2011. Relation between the North-Atlantic oscillation and hydroclimatic conditions in Mediterranean areas. Water Resour. Manage. 25 (5), 1269–1279. https://doi.org/10.1007/s11269-010-9742-5.
Cattani, E., Merino, A., Guijarro, J.A., Levizzani, V., 2018. East Africa rainfall trends and variability 1983–2015 using three long-term satellite products. Remote Sens. 10 (6), 931.
Clark, C.O., Webster, P.J., Cole, J.E., 2003. Interdecadal variability of the relationship between the Indian Ocean zonal mode and East African coastal rainfall anomalies. J. Clim. 16 (3), 548–554. https://doi.org/10.1175/1520-0442(2003)016<0548:ivotrb>2.0.co;2.
Clette, F., Svalgaard, L., Vaquero, J.M., Cliver, E.W., 2015. Revisiting the sunspot number. In: Balogh, A., Hudson, H., Petrovay, K., von Steiger, R. (Eds.), The Solar Activity Cycle: Physical Causes and Consequences. Springer New York, New York, NY, pp. 35–103. https://doi.org/10.1007/978-1-4939-2584-1_3.
Currie, R.G., 1993. Luni-solar 18.6- and 10–11-year solar cycle signals in South African rainfall. Int. J. Climatol. 13 (3), 237–256. https://doi.org/10.1002/joc.3370130302.
Dezfuli, A.K., Nicholson, S.E., 2013. The relationship of rainfall variability in Western Equatorial Africa to the tropical oceans and atmospheric circulation. Part II: the Boreal Autumn. J. Clim. 26 (1), 66–84. https://doi.org/10.1175/jcli-d-11-00686.1.
Diatta, S., Fink, A.H., 2014. Statistical relationship between remote climate indices and West African monsoon variability. Int. J. Climatol. 34 (12), 3348–3367. https://doi.org/10.1002/joc.3912.
Diem, J.E., Ryan, S.J., Hartter, J., Palace, M.W., 2014. Satellite-based rainfall data reveal a recent drying trend in central equatorial Africa. Clim. Change 126 (1), 263–272. https://doi.org/10.1007/s10584-014-1217-x.
Dunstone, N., et al., 2016. Skilful predictions of the winter North Atlantic oscillation one year ahead. Nat. Geosci. 9, 809. https://doi.org/10.1038/ngeo2824.
Easterbrook, D.J., 2016. Chapter 21 - using patterns of recurring climate cycles to predict future climate changes. In: Easterbrook, D.J. (Ed.), Evidence-Based Climate Science, second edition. Elsevier, pp. 395–411. https://doi.org/10.1016/B978-0-12-804588-6.00021-5.
Efron, B., Tibshirani, R.J., 1993. An introduction to the bootstrap. Monographs on Statistics and Applied Probability 57. Chapman & Hall, New York.
Eltahir, E.A.B., 1996. El Niño and the natural variability in the flow of the nile River. Water Resour. Res. 32 (1), 131–137. https://doi.org/10.1029/95wr02968.
Fer, I., Tietjen, B., Jeltsch, F., Wolff, C., 2017. The influence of El Niño–Southern oscillation regimes on eastern African vegetation and its future implications under the RCP8.5 warming scenario. Biogeosciences 14 (18), 4355–4374. https://doi.org/10.5194/bg-14-4355-2017.
Folland, C.K., Palmer, T.N., Parker, D.E., 1986. Sahel rainfall and worldwide sea temperatures, 1901–85. Nature 320 (6063), 602–607. https://doi.org/10.1038/320602a0.
Funk, C., 2011. We thought trouble was coming. Nature 476 (7). https://doi.org/10.1038/476007a.
Funk, C., et al., 2018. Examining the role of unusually warm Indo-Pacific sea-surface temperatures in recent African droughts. Q. J. R. Meteorolog. Soc. 144 (S1), 360–383. https://doi.org/10.1002/qj.3266.
Gachari, F., Mulati, D.M., Mutuku, J.N., 2014. Sunspot numbers: implications on Eastern African rainfall. S. Afr. J. Sci. 110, 1–5.
Gitau, W., Camberlin, P., Ogallo, L., Bosire, E., 2017. Trends of intraseasonal descriptors of wet and dry spells over equatorial eastern Africa. Int. J. Climatol. https://doi.org/10.1002/joc.5234.
Grinsted, A., Moore, J.C., Jevrejeva, S., 2004. Application of the cross wavelet transform and wavelet coherence to geophysical time series. Nonlin. Processes Geophys. 11 (5/6), 561–566. https://doi.org/10.5194/npg-11-561-2004.
Hamid, R.H., Marzouk, B.A., 2018. Forecasting the peak of the present solar activity cycle 24. NRIAG J. Astron. Geophys. 7 (1), 15–19. https://doi.org/10.1016/j.nrjag.2018.02.002.
Hathaway, D.H., Upton, L.A., 2016. Predicting the amplitude and hemispheric asymmetry of solar cycle 25 with surface flux transport. J. Geophys. Res.: Space Phys. 121 (11), 10. https://doi.org/10.1002/2016JA023190, 744-10,753.
Haywood, J.M., Jones, A., Bellouin, N., Stephenson, D., 2013. Asymmetric forcing from stratospheric aerosols impacts Sahelian rainfall. Nat. Clim. Change 3 (7), 660–665. https://doi.org/10.1038/nclimate1857.
He, D., Lin, P., Liu, H., Ding, L., Jiang, J., 2019. DLENSO: a deep learning ENSO forecasting model. PRICAI 2019: Trends in Artificial Intelligence. Springer International Publishing, Cham, pp. 12–23.
Heine, K., Völkel, J., 2011. Extreme floods around ad 1700 in the northern Namib Desert, Namibia, and in the Orange River catchment, South Africa - were they forced by a decrease of solar irradiance during the little ice age? Geographia Polonica 84, 61–80. https://doi.org/10.7163/GPol.2011.S1.5.
Helama, S., Holopainen, J., 2012. Spring temperature variability relative to the North Atlantic Oscillation and sunspots — a correlation analysis with a Monte Carlo implementation. Palaeogeogr. Palaeoclimatol. Palaeoecol. 326–328 (0), 128–134. https://doi.org/10.1016/j.palaeo.2012.02.013.
Hennekam, R., Jilbert, T., Schnetger, B., de Lange, G.J., 2014. Solar forcing of Nile discharge and sapropel S1 formation in the early to middle Holocene eastern Mediterranean. Paleoceanography 29 (5), 343–356. https://doi.org/10.1002/2013PA002553.
Hermanson, L., et al., 2014. Forecast cooling of the Atlantic subpolar gyre and associated impacts. Geophys. Res. Lett. 41 (14), 5167–5174. https://doi.org/10.1002/2014gl060420.
Hoell, A., Funk, C., 2014. Indo-Pacific sea surface temperature influences on failed consecutive rainy seasons over eastern Africa. Clim. Dyn. 43 (5), 1645–1660. https://doi.org/10.1007/s00382-013-1991-6.
Hoell, A., Funk, C., Barlow, M., 2014. La Niña diversity and Northwest Indian Ocean rim teleconnections. Clim. Dyn. 43 (9), 2707–2724. https://doi.org/10.1007/s00382-014-2083-y.
Hoell, A., Funk, C., Magadzire, T., Zinke, J., Husak, G., 2015. El Niño–Southern oscillation diversity and Southern Africa teleconnections during Austral Summer. Clim. Dyn. 45 (5), 1583–1599. https://doi.org/10.1007/s00382-014-2414-z.
Hoell, A., Funk, C., Zinke, J., Harrison, L., 2017. Modulation of the Southern Africa precipitation response to the El Niño Southern oscillation by the subtropical Indian Ocean Dipole. Clim. Dyn. 48 (7), 2529–2540. https://doi.org/10.1007/s00382-016-3220-6.
Huo, W.-J., Xiao, Z.-N., 2016. The impact of solar activity on the 2015/16 El Niño event. Atmos. Oceanic Sci. Lett. 9 (6), 428–435. https://doi.org/10.1080/16742834.2016.1231567.
Hurrell, J.W., Kushnir, Y., Ottersen, G., Visbek, M., 2003. An overview of the North Atlantic Oscillation. In: Hurrell, J.W., Kushnir, Y., Ottersen, G., Visbeck, M. (Eds.), The North Atlantic Oscillation: Climatic Significance and Environmental Impact. American Geophysical Union, Geophysical Monograph Series, pp. 1–35. https://doi.org/10.1029/134GM01. DOI.
Hutchinson, P., 1992. The Southern oscillation and prediction of "Der" season rainfall in Somalia. J. Clim. 5 (5), 525–531.
Indeje, M., Semazzi, F.H.M., Ogallo, L.J., 2000. ENSO signals in East African rainfall seasons. Int. J. Climatol. 20 (1), 19–46. https://doi.org/10.1002/(sici)1097-0088(200001)20:1<19::aid-joc449>3.0.co;2-0.
Junginger, A., Roller, S., Olaka, L.A., Trauth, M.H., 2014. The effects of solar irradiation changes on the migration of the Congo air boundary and water levels of paleo-Lake Suguta, Northern Kenya rift, during the African humid period (15–5ka BP). Palaeogeogr. Palaeoclimatol. Palaeoecol. 396, 1–16. https://doi.org/10.1016/j.palaeo.2013.12.007.
Kane, R.P., 2009. Periodicities, ENSO effects and trends of some South African rainfall series: an update. S. Afr. J. Sci. 105, 199–207.

Kantelhardt, J.W., Koscielny-Bunde, E., Rego, H.H.A., Havlin, S., Bunde, A., 2001. Detecting long-range correlations with detrended fluctuation analysis. Phys. A: Stat. Mech. Appl. 295 (3), 441–454. https://doi.org/10.1016/S0378-4371(01)00144-3.
Keenlyside, N.S., Latif, M., Jungclaus, J., Kornblueh, L., Roeckner, E., 2008. Advancing decadal-scale climate prediction in the North Atlantic sector. Nature 453, 84–88.
Kerr, R.A., 2000. A North Atlantic climate pacemaker for the centuries. Science 288 (5473), 1984–1985. https://doi.org/10.1126/science.288.5473.1984.
Kiladis, G.N., Diaz, H.F., 1989. Global climatic anomalies associated with extremes in the Southern oscillation. J. Clim. 2 (9), 1069–1090. https://doi.org/10.1175/1520-0442(1989)002<1069:gcaawe>2.0.co;2.
Kirov, B., Georgieva, K., 2002. Long-term variations and interrelations of ENSO, NAO and solar activity. Phys. Chem. Earth Parts A/B/C 27 (6), 441–448. https://doi.org/10.1016/S1474-7065(02)00024-4.
Klöwer, M., Latif, M., Ding, H., Greatbatch, R.J., Park, W., 2014. Atlantic meridional overturning circulation and the prediction of North Atlantic sea surface temperature. Earth. Planet. Sci. Lett. 406, 1–6. https://doi.org/10.1016/j.epsl.2014.09.001.
Knight, J.R., Folland, C.K., Scaife, A.A., 2006. Climate impacts of the Atlantic Multidecadal Oscillation. Geophys. Res. Lett. 33 (17) https://doi.org/10.1029/2006gl026242.
Knippertz, P., Christoph, M., Speth, P., 2003a. Long-term precipitation variability in Morocco and the link to the large-scale circulation in recent and future climates. Meteorol. Atmos. Phys. 83 (1), 67–88. https://doi.org/10.1007/s00703-002-0561-y.
Knippertz, P., Ulbrich, U., Marques, F., Corte-Real, J., 2003b. Decadal changes in the link between El Niño and springtime North Atlantic Oscillation and European–North African rainfall. Int. J. Climatol. 23 (11), 1293–1311. https://doi.org/10.1002/joc.944.
Knudsen, M.F., Jacobsen, B.H., Seidenkrantz, M.-S., Olsen, J., 2014. Evidence for external forcing of the Atlantic Multidecadal Oscillation since termination of the little ice age. Nat. Commun. 5, 3323. https://doi.org/10.1038/ncomms4323.
Kodera, K., 2002. Solar cycle modulation of the North Atlantic Oscillation: implication in the spatial structure of the NAO. Geophys. Res. Lett. 29 (8), 59–1–59–4. https://doi.org/10.1029/2001GL014557.
Kodera, K., 2005. Possible solar modulation of the ENSO cycle. Pap. Meteorol. Geophys. 55 (1+2), 21–32. https://doi.org/10.2467/mripapers.55.21.
Kodera, K., Coughlin, K., Arakawa, O., 2007. Possible modulation of the connection between the Pacific and Indian Ocean variability by the solar cycle. Geophys. Res. Lett. 34 (3) https://doi.org/10.1029/2006gl027827.
Köppen, W., 1918. Klassification der Klimate nach Temperatur, Niederschlag and Jahreslauf. Petermanns Geographische Mitteilungen, 64. pp.
Korecha, D., Barnston, A.G., 2007. Predictability of june–september rainfall in Ethiopia. Mon. Weather Rev. 135 (2), 628–650. https://doi.org/10.1175/mwr3304.1.
Lamb, P.J., Peppler, R.A., 1987. North Atlantic Oscillation: concept and an application. Bull. Am. Meteorol. Soc. 68 (10), 1218–1225. https://doi.org/10.1175/1520-0477(1987)068<1218:naocaa>2.0.co;2.
Laurenz, L., Lüdecke, H.-J., Lüning, S., 2019. Influence of solar activity changes on European rainfall. J. Atmos. Sol. Terr. Phys. 185, 29–42. https://doi.org/10.1016/j.jastp.2019.01.012.
Li, S., Robinson, W.A., Peng, S., 2003. Influence of the North Atlantic SST tripole on northwest African rainfall. J. Geophys. Res.: Atmos. 108 (D19) https://doi.org/10.1029/2002JD003130.
Li, H., Wang, H., Yin, Y., 2012. Interdecadal variation of the West African summer monsoon during 1979–2010 and associated variability. Clim. Dyn. 39 (12), 2883–2894. https://doi.org/10.1007/s00382-012-1426-9.
Li, J., Sun, C., Jin, F.-F., 2013. NAO implicated as a predictor of Northern Hemisphere mean temperature multidecadal variability. Geophys. Res. Lett. 40 (20), 5497–5502. https://doi.org/10.1002/2013gl057877.
Liebmann, B., et al., 2014. Understanding recent Eastern Horn of Africa rainfall variability and change. J. Clim. 27 (23), 8630–8645. https://doi.org/10.1175/jcli-d-13-00714.1.
Lim, E.-P., Hendon, H.H., 2017. Causes and predictability of the negative Indian Ocean Dipole and its impact on La Niña during 2016. Sci. Rep. 7 (1), 12619 https://doi.org/10.1038/s41598-017-12674-z.
Linderholm, H.W., Folland, C.K., Walther, A., 2009. A multicentury perspective on the summer North Atlantic Oscillation (SNAO) and drought in the eastern Atlantic region. J. Quat. Sci. 24 (5), 415–425. https://doi.org/10.1002/jqs.1261.
López-Moreno, J.I., et al., 2011. Effects of the North Atlantic Oscillation (NAO) on combined temperature and precipitation winter modes in the Mediterranean mountains: observed relationships and projections for the 21st century. Global Planet. Change 77 (1), 62–76. https://doi.org/10.1016/j.gloplacha.2011.03.003.
Losada, T., et al., 2012. Tropical SST and Sahel rainfall: a non-stationary relationship. Geophys. Res. Lett. 39 (12) https://doi.org/10.1029/2012GL052423.
Lott, F.C., Christidis, N., Stott, P.A., 2013. Can the 2011 East African drought be attributed to human-induced climate change? Geophys. Res. Lett. 40 (6), 1177–1181. https://doi.org/10.1002/grl.50235.
Lüdecke, H.-J., Cina, R., Dammschneider, H.-J., Lüning, S., 2020. Decadal and multidecadal natural variability in European temperature. J. Atmos. Sol. Terr. Phys. 205, 105294 https://doi.org/10.1016/j.jastp.2020.105294.
Lüning, S., Gałka, M., Danladi, I.B., Adagunodo, T.A., Vahrenholt, F., 2018. Hydroclimate in Africa during the medieval climate anomaly. Palaeogeogr. Palaeoclimatol. Palaeoecol. 495, 309–322.
Luo, J., Ying, K., He, P., Bai, J., 2005. Properties of Savitzky–Golay digital differentiators. Digital Signal Process. 15 (2), 122–136. https://doi.org/10.1016/j.dsp.2004.09.008.
Lyon, B., DeWitt, D.G., 2012. A recent and abrupt decline in the East African long rains. Geophys. Res. Lett. 39 (2) https://doi.org/10.1029/2011GL050337. L02702.
MacKellar, N., New, M., Jack, C., 2014. Observed and modelled trends in rainfall and temperature for South Africa: 1960–2010. S. Afr. J. Sci. 110 (7/8), 13. https://doi.org/10.1590/sajs.2014/20130353.
Malik, A., Brönnimann, S., Perona, P., 2018. Statistical link between external climate forcings and modes of ocean variability. Clim. Dyn. 50 (9), 3649–3670. https://doi.org/10.1007/s00382-017-3832-5.
Manatsa, D., Behera, S.K., 2013. On the epochal strengthening in the relationship between rainfall of East Africa and IOD. J. Clim. 26 (15), 5655–5673. https://doi.org/10.1175/jcli-d-12-00568.1.
Manatsa, D., Mukwada, G., 2012. rainfall mechanisms for the dominant rainfall Mode over Zimbabwe relative to ENSO and/or IODZM. Sci. World J. 2012, 926310 https://doi.org/10.1100/2012/926310.
Manatsa, D., Reason, C.J.C., Mukwada, G., 2012. On the decoupling of the IODZM from southern Africa summer rainfall variability. Int. J. Climatol. 32 (5), 727–746. https://doi.org/10.1002/joc.2306.
Mantua, N.J., Hare, S.R., 2002. The Pacific decadal oscillation. J. Oceanogr. 58 (1), 35–44. https://doi.org/10.1023/A:1015820616384.
Mantua, N.J., Hare, S.R., Zhang, Y., Wallace, J.M., Francis, R.C., 1997. A Pacific interdecadal climate oscillation with impacts on salmon production. Bull. Am. Meteorol. Soc. 78 (6), 1069–1079.
Marchane, A., Jarlan, L., Boudhar, A., Tramblay, Y., Hanich, L., 2016. Linkages between snow cover, temperature and rainfall and the North Atlantic Oscillation over Morocco. Clim. Res. 69 (3), 229–238.
Marchant, R., Mumbi, C., Behera, S., Yamagata, T., 2007. The Indian Ocean dipole – the unsung driver of climatic variability in East Africa. Afr. J. Ecol. 45 (1), 4–16. https://doi.org/10.1111/j.1365-2028.2006.00707.x.
Martin, E.R., Thorncroft, C.D., 2014. The impact of the AMO on the West African monsoon annual cycle. Q. J. R. Meteorolog. Soc. 140 (678), 31–46. https://doi.org/10.1002/qj.2107.
Martin, E.R., Thorncroft, C., Booth, B.B.B., 2014. The multidecadal Atlantic SST—Sahel rainfall teleconnection in CMIP5 simulations. J. Clim. 27 (2), 784–806. https://doi.org/10.1175/jcli-d-13-00242.1.
Maruyama, F., Kai, K., Morimoto, H., 2017. Wavelet-based multifractal analysis on a time series of solar activity and PDO climate index. Adv. Space Res. 60 (6), 1363–1372. https://doi.org/10.1016/j.asr.2017.06.004.
Masih, I., Maskey, S., Mussá, F.E.F., Trambauer, P., 2014. A review of droughts on the African continent: a geospatial and long-term perspective. Hydrol. Earth Syst. Sci. 18 (9), 3635–3649. https://doi.org/10.5194/hess-18-3635-2014.

Mason, S.J., Goddard, L., 2001. Probabilistic precipitation anomalies associated with EN SO. Bull. Am. Meteorol. Soc. 82 (4), 619–638. https://doi.org/10.1175/1520-0477(2001)082<0619:ppaawe>2.3.co;2.
Mason, S.J., Tyson, P.D., 1992. The modulation of sea surface temperature and rainfall associations over southern Africa with solar activity and the quasi-biennial oscillation. J. Geophys. Res.: Atmos. 97 (D5), 5847–5856. https://doi.org/10.1029/91jd02189.
McDonald, J.H., 2014. Handbook of Biological Statistics. Sparky House Publishing, Baltimore, MD.
McHugh, M.J., Rogers, J.C., 2001. North Atlantic Oscillation influence on precipitation variability around the Southeast African convergence zone. J. Clim. 14 (17), 3631–3642. https://doi.org/10.1175/1520-0442(2001)014<3631:naoiop>2.0.co;2.
Meddi, M.M., Assani, A.A., Meddi, H., 2010. Temporal variability of annual rainfall in the Macta and Tafna catchments, northwestern Algeria. Water Resour. Manage. 24 (14), 3817–3833. https://doi.org/10.1007/s11269-010-9635-7.
Mohino, E., Janicot, S., Bader, J., 2011. Sahel rainfall and decadal to multi-decadal sea surface temperature variability. Clim. Dyn. 37 (3), 419–440. https://doi.org/10.1007/s00382-010-0867-2.
Mpelasoka, F., Awange, J.L., Zerihun, A., 2018. Influence of coupled ocean-atmosphere phenomena on the Greater Horn of Africa droughts and their implications. Sci. Total Environ. 610-611, 691–702. https://doi.org/10.1016/j.scitotenv.2017.08.109.
Muthers, S., Raible, C.C., Rozanov, E., Stocker, T.F., 2016. Response of the AMOC to reduced solar radiation – the modulating role of atmospheric chemistry. Earth Syst. Dynam. 7 (4), 877–892. https://doi.org/10.5194/esd-7-877-2016.
Nash, D.J., et al., 2016. African hydroclimatic variability during the last 2000 years. Quat. Sci. Rev. 154, 1–22.
Nicholson, S.E., 2000. The nature of rainfall variability over Africa on time scales of decades to millenia. Global Planet. Change 26 (1–3), 137–158. https://doi.org/10.1016/S0921-8181(00)00040-0.
Nicholson, S.E., 2014. Spatial teleconnections in African rainfall: a comparison of 19th and 20th century patterns. Holocene 24 (12), 1840–1848. https://doi.org/10.1177/0959683614551230.
Nicholson, S.E., 2015. Long-term variability of the East African 'short rains' and its links to large-scale factors. Int. J. Climatol. 35 (13), 3979–3990. https://doi.org/10.1002/joc.4259.
Nicholson, S.E., 2017. Climate and climatic variability of rainfall over eastern Africa. Rev. Geophys. 55 (3), 590–635. https://doi.org/10.1002/2016rg000544.
Nicholson, S.E., Kim, J., 1997. The relationship of the El Nino-Southern oscillation to African rainfall. Int. J. Climatol. 17 (2), 117–135. https://doi.org/10.1002/(sici)1097-0088(199702)17:2<117::aid-joc84>3.0.co;2-o.
Nicholson, S.E., Funk, C., Fink, A.H., 2018. Rainfall over the African continent from the 19th through the 21st century. Global Planet. Change 165, 114–127. https://doi.org/10.1016/j.gloplacha.2017.12.014.
Nieto-Moreno, V., et al., 2015. Palaeoclimate and palaeoceanographic conditions in the westernmost Mediterranean over the last millennium: an integrated organic and inorganic approach. J. Geol. Soc. 172 (2), 264–271. https://doi.org/10.1144/jgs2013-105.
Nouaceur, Z., Murarescu, O., 2016. Rainfall variability and trend analysis of annual rainfall in North Africa. Int. J. Atmos. Sci. 2016, 12. https://doi.org/10.1155/2016/7230450.
Nugroho, J.T., 2007. Appearance of solar activity signals in Indian Ocean Dipole (IOD) phenomena and monsoon climate pattern over Indonesia. Bull. Astron. Soc. India 35, 575–579.
O'Reilly, C.H., Woollings, T., Zanna, L., 2017. The dynamical influence of the Atlantic Multidecadal Oscillation on continental climate. J. Clim. 30 (18), 7213–7230. https://doi.org/10.1175/jcli-d-16-0345.1.
Ogallo, L.J., 1988. Relationships between seasonal rainfall in East Africa and the Southern oscillation. J. Climatol. 8 (1), 31–43. https://doi.org/10.1002/joc.3370080104.
Ogou, F.K., Yang, Q., Duan, Y., Ma, Z., 2019. Comparative analysis of interdecadal precipitation variability over central North China and sub Saharan Africa. Atmos. Oceanic Sci. Lett. 12 (3), 201–207. https://doi.org/10.1080/16742834.2019.1593040.
Ogwang, B.A., Ongoma, V., Xing, L., Ogou, K.F., 2015. Influence of Mascarene High and Indian Ocean dipole on East African extreme weather events. Geogr. Pannonica 19 (2), 64–72. https://doi.org/10.5937/GeoPan1502064O.
Otterå, O.H., Bentsen, M., Drange, H., Suo, L., 2010. External forcing as a metronome for Atlantic multidecadal variability. Nat. Geosci. 3, 688–694. https://doi.org/10.1038/NGEO955.
Otto, F.E.L., et al., 2018. Anthropogenic influence on the drivers of the Western Cape drought 2015–2017. Environ. Res. Lett. 13 (12) https://doi.org/10.1088/1748-9326/aae9f9, 124010.
Ouachani, R., Bargaoui, Z., Ouarda, T., 2013. Power of teleconnection patterns on precipitation and streamflow variability of upper Medjerda Basin. Int. J. Climatol. 33 (1), 58–76. https://doi.org/10.1002/joc.3407.
Owiti, Z., Ogallo, L.A., Mutemi, J., 2008. Linkages between the Indian Ocean dipole and East African seasonal rainfall anomalies. J. Kenya Meteorol. Soc. 2 (1), 3–17.
Park, J.-y., Bader, J., Matei, D., 2016. Anthropogenic Mediterranean warming essential driver for present and future Sahel rainfall. Nature Clim. Change 6 (10), 941–945. https://doi.org/10.1038/nclimate3065.
Petersik, P.J., Dijkstra, H.A., 2020. Probabilistic forecasting of El Niño using neural network models. Geophys. Res. Lett. 47 (6) https://doi.org/10.1029/2019gl086423 e2019GL086423.
Philippon, N., Rouault, M., Richard, Y., Favre, A., 2012. The influence of ENSO on winter rainfall in South Africa. Int. J. Climatol. 32 (15), 2333–2347. https://doi.org/10.1002/joc.3403.
Reason, C.J.C., 2001. Subtropical Indian Ocean SST dipole events and southern African rainfall. Geophys. Res. Lett. 28 (11), 2225–2227. https://doi.org/10.1029/2000gl012735.
Riley, K.F., Hobson, M.P., Bence, S.J., 2006. Mathematical Methods for Physics and Engineering: A Comprehensive Guide. Cambridge University Press, Cambridge. https://doi.org/10.1017/CBO9780511810763. DOI.
Roberts, N., et al., 2012. Palaeolimnological evidence for an east–west climate see-saw in the Mediterranean since AD 900. Global Planet. Change 84, 23–34. https://doi.org/10.1016/j.gloplacha.2011.11.002.
Rodó, X., Baert, E., Comín, F.A., 1997. Variations in seasonal rainfall in Southern Europe during the present century: relationships with the North Atlantic Oscillation and the El Niño-Southern oscillation. Clim. Dyn. 13 (4), 275–284. https://doi.org/10.1007/s003820050165.
Ropelewski, C.F., Halpert, M.S., 1987. Global and regional scale precipitation patterns associated with the El Niño/Southern oscillation. Mon. Weather Rev. 115 (8), 1606–1626. https://doi.org/10.1175/1520-0493(1987)115<1606:garspp>2.0.co;2.
Rowell, D.P., Booth, B.B.B., Nicholson, S.E., Good, P., 2015. Reconciling past and future rainfall trends over East Africa. J. Clim. 28 (24), 9768–9788. https://doi.org/10.1175/JCLI-D-15-0140.1.
Ruzmaikin, A., Feynman, J., Yung, Y.L., 2006. Is solar variability reflected in the Nile River? J. Geophys. Res.: Atmos. 111 (D21) https://doi.org/10.1029/2006jd007462.
Saji, N.H., Goswami, B.N., Vinayachandran, P.N., Yamagata, T., 1999. A dipole mode in the tropical Indian Ocean. Nature 401 (6751), 360–363.
Sánchez-López, G., et al., 2016. Climate reconstruction for the last two millennia in central Iberia: the role of East Atlantic (EA), North Atlantic Oscillation (NAO) and their interplay over the Iberian Peninsula. Quat. Sci. Rev. 149, 135–150. https://doi.org/10.1016/j.quascirev.2016.07.021.
Savitzky, A., Golay, M.J.E., 1964. Smoothing and differentiation of data by simplified least squares procedures. Anal. Chem. 36 (8), 1627–1639. https://doi.org/10.1021/ac60214a047.
Scaife, A.A., et al., 2014. Skillful long-range prediction of European and North American winters. Geophys. Res. Lett. 41 (7), 2514–2519. https://doi.org/10.1002/2014GL059637.
Schlesinger, M.E., Ramankutty, N., 1994. An oscillation in the global climate system of period 65–70 years. Nature 367 (6465), 723–726. https://doi.org/10.1038/367723a0.
Segele, Z.T., Lamb, P.J., Leslie, L.M., 2009. Large-scale atmospheric circulation and global sea surface temperature associations with Horn of Africa June–September rainfall. Int. J. Climatol. 29 (8), 1075–1100. https://doi.org/10.1002/joc.1751.

Shanahan, T.M., et al., 2009. Atlantic forcing of persistent drought in West Africa. Science 324 (5925), 377–380. https://doi.org/10.1126/science.1166352.
Smith, D.M., Scaife, A.A., Eade, R., Knight, J.R., 2016. Seasonal to decadal prediction of the winter North Atlantic Oscillation: emerging capability and future prospects. Q. J. R. Meteorolog. Soc. 142 (695), 611–617. https://doi.org/10.1002/qj.2479.
Stager, J.C., Cumming, B.F., Meeker, L.D., 2003. A 10,000-year high-resolution diatom record from Pilkington Bay, Lake Victoria, East Africa. Quat. Res. 59 (2), 172–181. https://doi.org/10.1016/S0033-5894(03)00008-5.
Stephenson, D.B., Wanner, H., Brönnimann, S., Luterbacher, J., 2003. The history of scientific research on the North Atlantic Oscillation. In: Hurrell, W., Kushnir, Y., Ottersen, G., Visbeck, M. (Eds.), The North Atlantic Oscillation: Climatic Significance and Environmental Impact, pp. 37–50. https://doi.org/10.1029/134gm02.
Sutton, R.T., Dong, B., 2012. Atlantic Ocean influence on a shift in European climate in the 1990s. Nat. Geosci. 5, 788. https://doi.org/10.1038/ngeo1595.
Taibi, S., Meddi, M., Mahé, G., Assani, A., 2017. Relationships between atmospheric circulation indices and rainfall in Northern Algeria and comparison of observed and RCM-generated rainfall. Theor. Appl. Climatol. 127 (1), 241–257. https://doi.org/10.1007/s00704-015-1626-4.
Taye, M.T., Willems, P., 2012. Temporal variability of hydroclimatic extremes in the Blue Nile basin. Water Resour. Res. 48 (3) https://doi.org/10.1029/2011WR011466.
Thiéblemont, R., Matthes, K., Omrani, N.-E., Kodera, K., Hansen, F., 2015. Solar forcing synchronizes decadal North Atlantic climate variability. Nat. Commun. 6, 8268. https://doi.org/10.1038/ncomms9268.
Tierney, J.E., Smerdon, J.E., Anchukaitis, K.J., Seager, R., 2013. Multidecadal variability in East African hydroclimate controlled by the Indian Ocean. Nature 493 (7432), 389–392.
Ting, M., Kushnir, Y., Li, C., 2014. North Atlantic multidecadal SST oscillation: external forcing versus internal variability. J. Mar. Syst. 133, 27–38. https://doi.org/10.1016/j.jmarsys.2013.07.006.
Toulmin, S., 1961. Foresight and Understanding: An Enquiry into the Aims of Science. Indiana University Press, Bloomington.
Trenberth, K.E., Shea, D.J., 2006. Atlantic hurricanes and natural variability in 2005. Geophys. Res. Lett. 33 (12) https://doi.org/10.1029/2006GL026894.
Turki, I., Laignel, B., Laftouhi, N., Nouaceur, Z., Zamrane, Z., 2016. Investigating possible links between the North Atlantic Oscillation and rainfall variability in Marrakech (Morocco). Arabian J. Geosci. 9 (3), 243. https://doi.org/10.1007/s12517-015-2174-z.
Ummenhofer, C.C., Gupta, A.S., England, M.H., Reason, C.J.C., 2009. Contributions of Indian Ocean Sea surface temperatures to enhanced East African rainfall. J. Clim. 22 (4), 993–1013. https://doi.org/10.1175/2008jcli2493.1.
van Loon, H., Meehl, G.A., Arblaster, J.M., 2004. A decadal solar effect in the tropics in July–August. J. Atmos. Sol. Terr. Phys. 66, 1767–1778.
Verschuren, D., Laird, K.R., Cumming, B.F., 2000. Rainfall and drought in equatorial east Africa during the past 1,100 years. Nature 403 (6768), 410–414. DOI. http://www.nature.com/nature/journal/v403/n6768/suppinfo/403410a0_S1.html.
Wallace, M.G., 2019. Application of lagged correlations between solar cycles and hydrosphere components towards sub-decadal forecasts of streamflows in the Western USA. Hydrol. Sci. J. 64 (2), 137–164. https://doi.org/10.1080/02626667.2019.1567925.
Wang, J., et al., 2017a. Internal and external forcing of multidecadal Atlantic climate variability over the past 1,200 years. Nat. Geosci. 10, 512. https://doi.org/10.1038/ngeo2962.
Wang, L., Ting, M., Kushner, P.J., 2017b. A robust empirical seasonal prediction of winter NAO and surface climate. Sci. Rep. 7 (1), 279. https://doi.org/10.1038/s41598-017-00353-y.
Williams, A.P., Funk, C., 2011. A westward extension of the warm pool leads to a westward extension of the Walker circulation, drying eastern Africa. Clim. Dyn. 37 (11), 2417–2435. https://doi.org/10.1007/s00382-010-0984-y.
Wyatt, M.G., Kravtsov, S., Tsonis, A.A., 2012. Atlantic Multidecadal Oscillation and Northern Hemisphere's climate variability. Clim. Dyn. 38 (5–6), 929–949.
Yamakawa, S., Inoue, M., Suppiah, R., 2016. Relationships between solar activity and variations in SST and atmospheric circulation in the stratosphere and troposphere. Quat. Int. 397, 289–299. https://doi.org/10.1016/j.quaint.2015.11.018.
Zaroug, M.A.H., Giorgi, F., Coppola, E., Abdo, G.M., Eltahir, E.A.B., 2014. Simulating the connections of ENSO and the rainfall regime of East Africa and the upper Blue Nile region using a climate model of the tropics. Hydrol. Earth Syst. Sci. 18 (11), 4311–4323. https://doi.org/10.5194/hess-18-4311-2014.
Zeroual, A., Assani, A.A., Meddi, M., 2016. Combined analysis of temperature and rainfall variability as they relate to climate indices in Northern Algeria over the 1972–2013 period. Hydrol. Res. 48 (2), 584–595. https://doi.org/10.2166/nh.2016.244.
Zhang, R., Delworth, T.L., 2006. Impact of Atlantic multidecadal oscillations on India/Sahel rainfall and Atlantic hurricanes. Geophys. Res. Lett. 33 (17) https://doi.org/10.1029/2006GL026267.
Zhang, Q., Holmgren, K., Sundqvist, H., 2015. Decadal rainfall dipole oscillation over Southern Africa modulated by variation of Austral summer land–Sea contrast along the East Coast of Africa. J. Atmos. Sci. 72 (5), 1827–1836. https://doi.org/10.1175/JAS-D-14-0079.1.
Zhang, R., et al., 2019. A review of the role of the Atlantic meridional overturning circulation in Atlantic multidecadal variability and associated climate impacts. Rev. Geophys. 57 (2), 316–375. https://doi.org/10.1029/2019rg000644.